

RESEARCH

Open Access



# Activation of central and peripheral transient receptor potential melastatin 8 increases susceptibility to spreading depolarization and facilitates trigeminal neuroinflammation

Tzu-Ting Liu<sup>1,2</sup>, Pin-Yu Chen<sup>3,4</sup>, Chyun-Yea Tseng<sup>2</sup>, Yun-Ning Chen<sup>2</sup>, Jian-Bang Chen<sup>2</sup>, Tz-Han Ni<sup>2</sup>, Shuu-Jiun Wang<sup>1,4,5</sup>, Shih-Pin Chen<sup>1,3,5,6</sup> and Jiin-Cherng Yen<sup>2\*</sup>

## Abstract

**Background** *Transient receptor potential melastatin 8 (TRPM8)*, a gene encoding a nonselective cation channel responsive to cold stimuli, has been implicated in migraine susceptibility. Despite this association, the role of TRPM8 to migraine pathogenesis remains elusive. This study aims to elucidate the potential role of TRPM8 in migraine pathophysiology.

**Methods** TRPM8 expression in the cortex and primary trigeminal ganglion (TG) cells was analyzed via immunostaining. The central role of TRPM8 was assessed using a spreading depolarization (SD) model, where intracerebroventricular injections or topical applications of TRPM8 agonists and antagonists were administered to rats to investigate their effects on KCl-evoked SD and SD-induced cortical inflammation. The peripheral role of TRPM8 in migraine was evaluated using primary cultures of rat TG cells by analyzing the effects of TRPM8 activation on calcitonin gene-related peptide (CGRP) expression, release, and trigeminal neuroinflammation.

**Results** TRPM8 was homogeneously distributed in the cerebral cortex, predominantly co-localizing with cortical neurons. Activation of cortical TRPM8 increased the frequency of KCl-evoked SD and exacerbated SD-induced cortical inflammation. Interestingly, inhibition of cerebral TRPM8 had negligible effects. In TG primary cultures, TRPM8 activation upregulated CGRP expression and release and induced cyclooxygenase-2 (Cox2) upregulation via a calmodulin kinase II (CaMKII)-dependent mechanism.

**Conclusions** TRPM8 activation increased susceptibility to SD and facilitated the effects of CGRP and trigeminal neuroinflammation, implicating that TRPM8 may contribute to migraine pathophysiology through central and peripheral mechanisms.

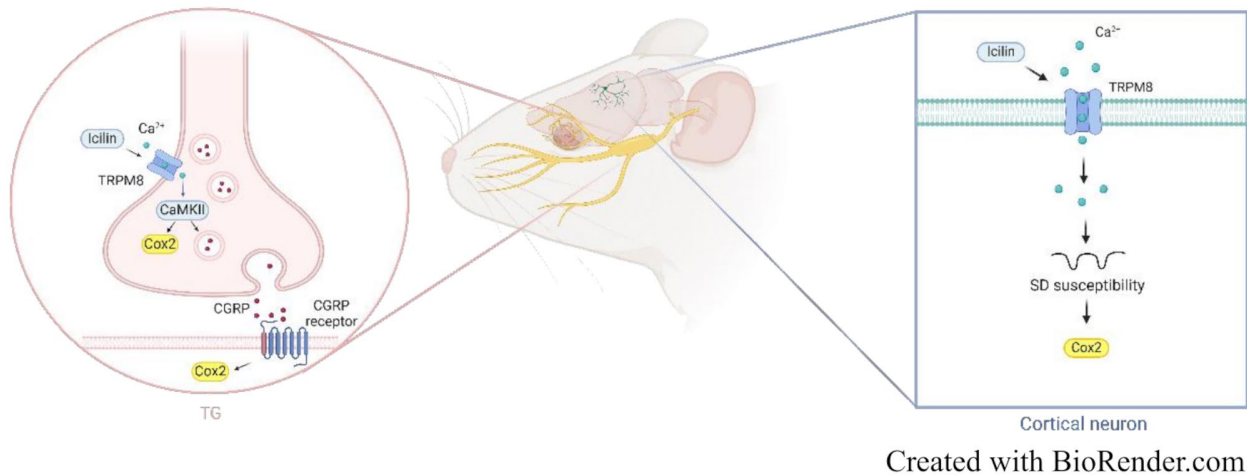
\*Correspondence:  
Jiin-Cherng Yen  
jcyen@nycu.edu.tw

Full list of author information is available at the end of the article



© The Author(s) 2025. **Open Access** This article is licensed under a Creative Commons Attribution-NonCommercial-NoDerivatives 4.0 International License, which permits any non-commercial use, sharing, distribution and reproduction in any medium or format, as long as you give appropriate credit to the original author(s) and the source, provide a link to the Creative Commons licence, and indicate if you modified the licensed material. You do not have permission under this licence to share adapted material derived from this article or parts of it. The images or other third party material in this article are included in the article's Creative Commons licence, unless indicated otherwise in a credit line to the material. If material is not included in the article's Creative Commons licence and your intended use is not permitted by statutory regulation or exceeds the permitted use, you will need to obtain permission directly from the copyright holder. To view a copy of this licence, visit <http://creativecommons.org/licenses/by-nc-nd/4.0/>.

### Graphical abstract



**Keywords** TRPM8, Spreading depolarization, Trigeminal ganglion, CGRP, Neuroinflammation

### Background

Migraine is characterized by recurrent, intense pulsating headaches, concomitant with symptoms such as nausea, vomiting, photophobia, and phonophobia. It ranks as the second leading cause of global disability [1], impacting approximately 15% of the population [2]. Genetic factors significantly influence migraine etiology, with genome-wide association studies (GWAS) revealing a correlation between migraine susceptibility and specific single nucleotide polymorphisms (SNPs) near the genetic loci of *transient receptor potential melastatin 8 (TRPM8)* [3–6]. TRPM8 is a non-selective cation channel that responds to temperatures below 26 °C and cooling substances like menthol. It is expressed in the primary afferent neurons of the trigeminal ganglia (TG) and dorsal root ganglia (DRG) [7, 8], dural afferent fibers [9], as well as cerebral vessels and brain parenchyma [10, 11]. These tissues are crucial for cooling sensation and pain perception, suggesting a potential causal role of TRPM8 in migraine pathophysiology [12].

Clinical studies have documented a potential association between migraines and exposure to cold, identifying cold weather and cold stimuli as potential triggers for migraine attacks [13]. Furthermore, individuals with migraines exhibit an increased susceptibility to cold-stimulus headaches [14, 15], often experiencing a higher pain intensity and a greater prevalence of associated symptoms when exposed to cold stimuli compared to healthy individuals [16]. Preclinical investigations further support TRPM8's involvement in migraine pathophysiology. Icilin-induced TRPM8 activation has been reported to cause cutaneous facial and hind paw cold allodynia in rats [17]. A study shows that genetic ablation of TRPM8

prevents nitroglycerin (NTG)-induced mechanical allodynia, suggesting that neurons expressing TRPM8 channels play a role in both spontaneous and evoked pain behaviors [18]. Conversely, clinical studies indicate that the topical cold therapy [19, 20], intranasal evaporative cooling [21], and cutaneous application of menthol [22] demonstrate efficacy against migraine attacks. Additionally, preclinical studies underscore TRPM8's protective role, as menthol has been found to alleviate migraine-related pain induced by topically applied inflammatory soup over the dura [23]. Moreover, TRPM8 expedites recovery from NTG-induced mechanical hypersensitivity in males [24]. Due to the controversial findings, the precise role of TRPM8 in migraine pathophysiology remains to be elucidated.

Spreading depolarization (SD), characterized by a slowly propagating wave of near-complete neuronal and glial depolarization, is considered the intrinsic mechanism underlying migraine aura [25, 26]. SD initiates cortical neuroinflammation and activates the trigemino-vascular system (TVS) [27–29], leading to the release of neuropeptides such as calcitonin gene-related peptide (CGRP) from meningeal nociceptors [30], which ultimately results in headaches. As a validated preclinical model of migraine, SD provides a robust platform for screening potential therapeutic targets and unraveling the intricate pathophysiology of migraine. This study focuses on examining the role of TRPM8 in susceptibility to migraines. Given its widespread distribution, we explored the functions of TRPM8 both centrally and peripherally. To elucidate the central effects, we first characterized the expression pattern of TRPM8 in the cerebral cortex and subsequently assessed its impact

on SD and the cortical inflammation. To evaluate the peripheral contribution, we utilized primary trigeminal neuronal cultures to investigate how TRPM8 activation affects CGRP expression and release, as well as neuroinflammation. Our study aims to explore the potential role of TRPM8 in migraine pathophysiology.

## Methods

### Ethics

Animal procedures were conducted following the ARRIVE guidelines. The research protocol received approval from the Institutional Animal Care and Use Committee at National Yang Ming Chiao Tung University, Taiwan.

### Animals

Male Sprague-Dawley rats, ranging in age from 6 to 8 weeks and weighing 200–350 g, sourced from BioLasco Taiwan, were employed for the SD model. Postnatal rats aged 8–10 days were selected for the establishment of primary TG cell cultures. Animals were housed in cages with environmental controls set to  $21 \pm 1$  °C for temperature, 40–70% for humidity, and a 12-hour light/dark cycle. Rats had *ad libitum* access to a rodent standard diet and water. To ensure proper acclimatization, all experiments commenced after a minimum acclimatization period of 3 days in these controlled environments.

### Surgery

Anesthesia was initially induced through an intraperitoneal injection of sodium pentobarbital (50 mg/kg). Simultaneously, a homeothermic system (Patterson Scientific, Waukesha, USA) was used to maintain the body temperature of the rats within the range of 36.8–37.2 °C. Following a tracheotomy to facilitate ventilation, mechanical ventilation was carried out using a ventilator (CWE, Ardmore, PA) delivering a gas mixture of 30% O<sub>2</sub> and 70% N<sub>2</sub>. To sustain anesthesia, polyethylene tubes (PE-50) were inserted into the femoral vein for intravenous infusion of sodium pentobarbital. The femoral artery was cannulated with PE-50, enabling continuous monitoring of systemic arterial pressure (Table 1) via a transducer

(T844, ADInstruments, Castle Hill, Australia). Heart rate was recorded from arterial pulses per minute (Table 1). Throughout the experimental procedure, a portable blood gas analyzer (Abbott, Princeton, USA) with single-use test cartridges was employed to monitor arterial pH, PaO<sub>2</sub>, and PaCO<sub>2</sub> (Table 1), ensuring the maintenance of the rats' normal physiological status.

The test agents were administered either via intracerebroventricular (i.c.v.) injection or topical application on the cerebral cortex. In the case of i.c.v. injection, rats were securely positioned in a stereotaxic apparatus. Craniotomies were performed to create three burr holes, enabling i.c.v. injection, SD induction, and recordings. The coordinates for the i.c.v. injection were 0.5 mm caudal and 1.5 mm lateral to the bregma, at a depth of 4 mm below the cortical surface, on the hemisphere contralateral to the SD induction site. For topical treatment, a cranial window ipsilateral to the SD side over the parietal cortex (AP: -1.5 mm, ML: 2 mm, diameter: 4 mm) was created, followed by the craniotomies for SD induction and recording.

### Pharmacological treatment

Anesthesia induction was used by intraperitoneal injection of sodium pentobarbital (50 mg/kg), and maintained through intravenous infusion of sodium pentobarbital at a rate of 15–20 mg/kg/h. For pharmacological treatment, rats were prepared for surgery as described above. In the case of i.c.v. injection, the TRPM8 agonist (icilin, 50–500 μM) or antagonist (M8-B, 5–50 μM) along with the vehicle (artificial cerebrospinal fluid with or without 0.1% DMSO), was administered to the lateral ventricle contralateral to the SD-induction side using a microinjection syringe (75RN SYR, 5 L from Hamilton) with a 32-gauge, 6 cm needle. The solutions were injected at a rate of 0.1 μl per 5 s, and the microinjection needle was gently removed at a rate of 0.8 mm per minute after 5 min. For topical treatment, a cranial window was pre-treated with a cotton ball soaked in the test drugs (M8-B, 50 μM) for 30 min before SD induction.

**Table 1** Animal physiology

Treatment	pH	PaCO <sub>2</sub>	PaO <sub>2</sub>	BP	HR
Vehicle (i.c.v.)	7.41 ± 0.03	39.0 ± 6.8	107.5 ± 13.3	116.1 ± 10.2	445.9 ± 29.7
Icilin (50 μM, i.c.v.)	7.40 ± 0.03	38.0 ± 5.9	105.0 ± 8.3	120.4 ± 8.4	419.0 ± 42.8
Icilin (500 μM, i.c.v.)	7.42 ± 0.03	36.4 ± 6.0	105.1 ± 13.5	108.2 ± 10.7	444.2 ± 55.0
aCSF (i.c.v.)	7.41 ± 0.03	39.5 ± 5.7	94.42 ± 11.1	112.4 ± 8.7	453.5 ± 33.3
M8-B (5 μM, i.c.v.)	7.40 ± 0.02	36.8 ± 6.7	101.9 ± 14.3	112.1 ± 6.8	412.9 ± 30.2
M8-B (50 μM, i.c.v.)	7.38 ± 0.03	41.1 ± 5.2	100.6 ± 8.0	112.4 ± 8.9	428.3 ± 41.3
Saline (topical)	7.42 ± 0.02	43.3 ± 3.6	110.9 ± 18.3	119.6 ± 14.4	366.9 ± 34.3
M8-B (topical)	7.42 ± 0.02	39.2 ± 2.7	102.1 ± 18.6	115.3 ± 12.0	427.1 ± 20.3

Data are presented as mean ± SD. All physiological parameters were maintained within normal range

### SD susceptibility

The methodology for susceptibility testing of SD adhered to our established protocols [31–33]. Initially, parietal bone exposure was meticulously performed, and two burr holes were drilled to enable SD recording (anteroposterior [AP]: bregma +2 mm, mediolateral [ML]: 2 mm; diameter: 1 mm, dura intact) and induction (AP: bregma –5 mm; ML: 2 mm; diameter: 1.5–2 mm, dura removed). An Ag/AgCl electrode, affixed to a glass capillary microelectrode, was positioned 0.5 mm below the cortical surface to record the direct current (DC) potential, which was subsequently amplified using an appropriate amplifier. An SD event was identified by a current shift exceeding 5 mV. The effects of TRPM8 on SD frequency, duration, and amplitude were evaluated.

### Primary culture of TG neurons

We adapted a previously established protocol for primary neuronal cultures with modifications [34]. Neonatal rats aged P8-P10 were anesthetized with sodium pentobarbital (50 mg/kg) and euthanized via transcardial perfusion. The skull and cerebrum were removed to isolate the TG. The collected tissue was washed with ice-cold Dulbecco's Modified Eagle Medium (DMEM) containing 1% penicillin-streptomycin. TG tissues were then transferred to a culture dish, dissected into small pieces (approximately 0.5 mm), and the supernatants were discarded. To eliminate calcium and magnesium interference during the enzymatic digestion, the TG tissue was rinsed twice with sterile phosphate-buffered saline (PBS). The tissue was then incubated in collagenase (2 mg/ml) at 37 °C for 45 min. After removing the supernatants, the tissue was resuspended in a mixture of neurobasal medium, N2 and B-27 supplements, basic fibroblast growth factor (bFGF), brain-derived neurotrophic factor (BDNF), glial cell-derived neurotrophic factor (GDNF), L-glutamine, and penicillin-streptomycin (for concentration, see Table 2). The tissue fragments were filtered through a 40 µm cell strainer twice, and the cell suspension was centrifuged at 1000 rpm for 5 min. After discarding the supernatants, the cells were uniformly seeded onto 24-well plates pre-coated with poly-ornithine and laminin in DMEM to ensure normal cell proliferation and cell-cell communication. The cultures were maintained in a humidified 37 °C incubator with 5% CO<sub>2</sub>, and the medium was replenished daily with cytosine-β-D-arabinofuranoside until the cells were ready for experimentation.

### Measurement of intracellular Ca<sup>2+</sup> concentration

Due to the limited number of cells obtained from a single TG, we pooled TG tissues from 2 to 3 animals, which were then subjected to the primary culture procedures mentioned above, followed by a previously established method to measure intracellular Ca<sup>2+</sup> levels [35]. Primary

TG cells were plated onto coverslips pre-coated with gelatin and then incubated with Fura-2 AM, a calcium fluorescent indicator, for 1 h at room temperature in the dark. After incubation, the dye solution was removed, and the cells were rinsed twice with HEPES-buffered saline. To facilitate the de-esterification of Fura-2 AM, the cells were further incubated with loading buffer supplemented with probenecid (2.5 mM) for a minimum of 20 min at room temperature. Intracellular Ca<sup>2+</sup> concentrations were quantified by measuring the fluorescence emission intensity at 510 nm, in response to 340 nm (for Ca<sup>2+</sup>-bound Fura-2) and 380 nm (for Ca<sup>2+</sup>-unbound Fura-2) excitation wavelengths at 2-second intervals. Excitation wavelength adjustment was performed using an ultra-fast switching monochromator (Polychrome V, TILL Photonics GmbH, Gräfelfing, Germany), and fluorescence signals were captured with a CCD camera (Micromax YHS1300, Roper Scientific, Trenton, NJ, USA) attached to a fluorescence microscope (IX70, Olympus, Tokyo, Japan). The change in the 340/380 nm excitation ratio over time was plotted to assess the variation in intracellular Ca<sup>2+</sup> levels. For the analysis of intracellular Ca<sup>2+</sup> dynamics, phase contrast and pseudocolor images were obtained for each experiment. Individual cells were manually outlined in the images, and the F340 nm/F380 nm ratios, representing Ca<sup>2+</sup>-bound and Ca<sup>2+</sup>-unbound Fura-2 fluorescence signals, were measured for each cell over time. The average ratio for each cell was calculated across the time course of the experiment. To determine the overall response in each independent experiment, the data from all cells within the experiment were averaged. Subsequently, the average values from each independent experiment were used to calculate the final group mean for each condition. To determine the percentage of responding cells, cells that showed a significant increase in the F340 nm/F380 nm ratio following treatment were considered responders. A response was defined as a ≥ 10% increase in the F340/F380 ratio relative to baseline values. The number of responding cells was counted and divided by the total number of cells analyzed in each independent experiment to obtain the proportion of responding cells. This proportion was then averaged across independent experiments to derive the final percentage of responding cells for each condition.

### Measurement of extracellular CGRP

The culture medium was collected and centrifuged at 5000×g for 5 min at 4 °C. Extracellular CGRP levels in the supernatant were assessed using a commercially available CGRP ELISA kit (details provided in Table 2), following the manufacturer's instructions. To investigate the role of extracellular Ca<sup>2+</sup>, we substituted Ca<sup>2+</sup>-free culture medium for the normal culture medium using the Ca<sup>2+</sup> chelator BAPTA for 5 min, followed by treatment with

**Table 2** Key resources

Reagent or resource type	Source	Identifier	Dilution/Application
Experimental models: Organisms/strains			
Rattus norvegicus: Sprague-Dawley (6–8 weeks old, male)	BioLASCO	RRID: RGD_737903	N/A
Rattus norvegicus: Sprague-Dawley (P8-P10 pups)	BioLASCO	RRID: RGD_737903	N/A
Antibodies			
Rabbit polyclonal anti-TRPM8	Alomone Labs	Cat #ACC-049; RRID: AB_2040254	1:1000 (WB) 1:100 (IF) 1:400 (ICC)
Rabbit polyclonal anti-Cox2	Abcam	Cat #ab15191; RRID: AB_2085144	1:1000 (tissue WB) 1:600 (cell WB) 1:200 (ICC)
Rabbit polyclonal anti-TNF- $\alpha$	Abcam	Cat #ab9739 RRID: AB_308774	1:250 (WB)
Mouse monoclonal anti-phospho-CaMKII Thr286 (clone 22B1)	Upstate	Cat # 05-533; RRID: AB_309788	1:400 (WB)
Rabbit monoclonal anti-CaMKII	Cell Signaling Technology	Cat #4436; RRID: AB_10545451	1:200 (WB)
Mouse monoclonal anti- $\alpha$ -tubulin (clone B512)	Sigma-Aldrich	Cat #T5168; RRID: AB_477579	1:5000 (WB)
Mouse monoclonal anti- $\beta$ -actin (clone-CA-15)	Sigma-Aldrich	Cat #TA5441; RRID: AB_476744	1:5000 (WB)
Mouse monoclonal anti-GAPDH	Abcam	Cat #ab8245 RRID: AB_2107448	1:5000 (WB)
Rabbit polyclonal anti-CGRP	Abcam	Cat #ab47027; RRID: AB_1141573	1:200 (ICC)
Mouse monoclonal anti-NeuN	Chemicon	Cat #MAB377; RRID: AB_2298772.	1:100 (IF) 1:200 (ICC)
Mouse monoclonal anti- $\beta$ III tubulin	Abcam	Cat #ab78078 RRID: AB_2256751	1:400 (ICC)
Mouse monoclonal anti-GFAP (clone GA5)	Sigma-Aldrich	Cat # G3893; RRID: AB_477010	1:100 (IF)
Goat polyclonal anti-Iba1	Abcam	Cat # ab5076; RRID: AB_2224402	1:100 (IF)
Donkey anti-rabbit IgG, HRP-linked	Cytiva	Cat #NA934; RRID: AB_772206	1:2500 (WB)
Sheep anti-mouse IgG, HRP Linked	Cytiva	Cat#NA931; RRID: AB_772210	1:2500 (WB)
Goat anti-rabbit IgG highly cross-adsorbed secondary antibody, Alexa Fluor 488	Invitrogen	Cat#A-11,034; RRID: AB_2576217	1:200 (IF) 1:500 (ICC)
Goat anti-mouse IgG cross-adsorbed secondary antibody, Alexa Fluor 488	Invitrogen	Cat#A-11,001; RRID: AB_2534069	1:200 (IF) 1:500 (ICC)
Goat anti-rabbit IgG cross-adsorbed secondary antibody, Alexa Fluor 594	Invitrogen	Cat#A-11,012; RRID: AB_141359	1:200 (IF) 1:500 (ICC)
Donkey anti-rabbit IgG highly cross-adsorbed secondary antibody, Alexa Fluor 594	Invitrogen	Cat#A-21,207 RRID: AB_141637	1:200 (IF)
Donkey anti-mouse IgG highly cross-adsorbed secondary antibody, Alexa Fluor 488	Invitrogen	Cat#A-21,202 RRID: AB_141607	1:200 (IF)
Donkey anti-rabbit IgG highly cross-adsorbed secondary antibody, Alexa Fluor 488	Invitrogen	Cat#A-21,206 RRID: AB_2535792	1:200 (IF)
Donkey anti-goat IgG cross-adsorbed secondary antibody, Alexa Fluor 594	Invitrogen	Cat# A-11,058; RRID: AB_142540	1:200 (IF)
Chemicals, culture medium, and recombinant proteins			
Icilin	Sigma Aldrich	Cat# I9532	50 and 500 $\mu$ M (in vivo) 0.1, 1, and 10 Mm (in vitro)
M8 B hydrochloride	Tocris	Cat#5324	50 $\mu$ M (in vivo)
KN 93	Tocris	Cat#1278	5 $\mu$ M (in vitro)

**Table 2** (continued)

Reagent or resource type	Source	Identifier	Dilution/Application
BIBN4096	R&D Systems	Cat #4561	1–10 nM (in vitro)
Fura-2 AM	Invitrogen	Cat#F1221	5 $\mu$ M (in vitro)
1,2-Bis(2-aminophenoxy)ethane-N, N,N',N'-tetraacetic acid (BAPTA)	Sigma Aldrich	Cat#14,510	20 mM (in vitro)
Neurobasal medium	Gibco	Cat#21,103,049	N/A
N-2 Supplement (100X)	Gibco	Cat#17,502,048	1X (primary culture)
B-27 Plus Supplement (50X)	Gibco	Cat#A3582801	1X (primary culture)
Rat FGF-basic (bFGF) recombinant protein	Gibco	Cat#400–29	20 ng/ $\mu$ L (primary culture)
Rat BDNF recombinant protein	Gibro	Cat#450-02	10 ng/ $\mu$ L (primary culture)
Rat GDNF recombinant protein	Gibro	Cat#450–51	10 ng/ $\mu$ L (primary culture)
Cytosine- $\beta$ -D-arabinofuranoside	Sigma Aldrich	Cat#C1768	3 $\mu$ M (primary culture)
L-glutamine	Biological Industries	Cat#03-020-1B	0.5 mM (primary culture)
poly-ornithine	R&D Systems	Cat#3436-100-01	50 $\mu$ g/mL (primary culture)
laminin	R&D Systems	Cat#3400-010-02	10 ng/ $\mu$ L (primary culture)
DPX Mountant for histology	Sigma Aldrich.	Cat#06522	N/A
Antifade Mounting Medium with DAPI	Vector Laboratories	Cat#H1500	N/A
Critical commercial assays			
CGRP (rat) EIA Kit	Cayman Chemical	Cat#589,001	N/A
ABC-HRP Kit, Peroxidase (Rabbit IgG)	Vector Laboratories	Cat#PK-6101	N/A
DAB Substrate Kit, Peroxidase (HRP), with Nickel	Vector Laboratories	Cat#SK-4100	N/A
Software and algorithms			
LabChart (Version 8)	ADInstruments	<a href="https://www.adinstruments.com/">https://www.adinstruments.com/</a>	N/A
FV10-ASW4.0	Olympus	<a href="https://www.olympus-lifescience.com/">https://www.olympus-lifescience.com/</a>	N/A
MShot Image Analysis System	MSHOT	<a href="https://www.m-shot.com/">https://www.m-shot.com/</a>	N/S
Graphpad Prism (Version 7)	GraphPad	<a href="https://www.graphpad.com/">https://www.graphpad.com/</a>	N/A
BioRender	BioRender	<a href="https://www.biorender.com/">https://www.biorender.com/</a>	N/A

vehicle or icilin for 30 min. Finally, the CGRP levels in the medium were measured using the ELISA kit.

### Immunohistochemistry

In accordance with established protocols [33, 36], rats were subjected to transcardial perfusion with a freshly prepared 4% paraformaldehyde during the tissue harvest. Following this, the brains were promptly harvested and post-fixed with 4% paraformaldehyde at 4 °C for 24 h. Subsequent to post-fixation, the brains underwent dehydration using a 30% sucrose solution (in 0.1 M PBS). Using a Thermo CryoStat NX50 cryostat, 20- $\mu$ m-thick cryoprotected cortical tissue sections were obtained. The cortical sections (bregma +1 to -3 mm) were rinsed in PBS to remove any residual O.C.T. After quenching endogenous peroxidase activity with 3% H<sub>2</sub>O<sub>2</sub>, sections underwent permeabilization and blocking using 3% normal serum in PBS (containing 0.375% gelatin and 0.2% triton-X-100) for a minimum of 60 min at room temperature. Primary antibodies (as outlined in Table 2) were applied to the sections, which were then incubated at 4 °C

for 24–48 h. Following PBS rinse, sections were probed with goat anti-rabbit biotinylated secondary antibody (Table 2) at room temperature for 1 h, followed by conjugation with avidin-biotin complex (Table 2) for 30 min at room temperature. Chromogenic detection was performed using DAB (3,3-diaminobenzidine) with nickel (Table 2). After staining, the sections were mounted onto silane-coated slides and dehydrated with graded ethanol concentrations of 50%, 75%, 95%, and 100%. For clearing, sections were treated with a 50% xylene in ethanol solution, followed by 100% xylene. Clearing is an important step in histopathology that helps remove dehydrating agents from tissues, making them transparent for improved tissue imaging. Xylene is widely used as a clearing agent due to its effectiveness in removing alcohols from tissues, facilitating paraffin infiltration, and enhancing tissue transparency for better visualization in light microscopy [37]. Image acquisition utilized an optical microscope (Olympus BX63, Tokyo, Japan) within a view area of 560  $\mu$ m $\times$ 400  $\mu$ m at 40X, 100X, or 400X magnification following coverslipping. The resultant images were

subjected to analysis utilizing the MShot Image Analysis system.

### Immunofluorescence staining

For multi-color staining in cortical sections, the sample preparation followed the our established immunohistochemistry protocol [31, 33, 36]. After permeabilization and blocking with a solution comprising 3% normal serum, 0.375% gelatin, and 0.2% Triton-X-100 in PBS, the sections underwent incubation with primary antibodies derived from distinct species (Table 2) at 4 °C for a duration of 24–48 h. Following this, the sections were treated with Alexa Fluor dye-conjugated secondary antibodies (Table 2) for a two-hour period at room temperature. Subsequent to this incubation, the tissue sections were stained with 600 nM DAPI for 10 min and meticulously washed with PBS to eliminate any residual fluorescent dye. Upon mounting on silane-coated slides and coverslipping with antifade mounting medium, the captured images were observed using a confocal laser scanning microscope (Olympus FV1000, Tokyo, Japan) within a view area of 200  $\mu\text{m}$   $\times$  200  $\mu\text{m}$  at 600X magnification. A uniform fluorescence threshold was consistently applied to all images within the same experimental group for subsequent image analysis through the utilization of ImageJ software. We quantified the number of DAPI-positive, NeuN-positive, and TRPM8-positive cells. The ratio of NeuN+/DAPI was calculated to represent the proportion of neurons among all cells. The ratio of TRPM8+/DAPI was calculated to represent the proportion of TRPM8-positive cells among all cells. Additionally, the ratio of TRPM8+NeuN+/NeuN+ was calculated to represent the proportion of TRPM8-positive neurons among all neurons.

### Western blot analysis

The protocol followed our established procedures [31, 33, 36]. We collected cortical samples situated 1 mm from the SD induction site and between the SD recording sites. These samples were promptly frozen for subsequent protein expression analysis. Upon thawing, the frozen samples were resuspended in lysis buffer (G Bioscience, Saint Louis, USA) supplemented with 10% (v/v) protease and phosphatase inhibitors (Roche, Mannheim, Germany) and homogenized. Following homogenization, the mixture underwent centrifugation at 4 °C, 10,000 $\times$ g for 15 min. The protein concentration in the cell lysates was determined using the Bradford assay [38], following the manufacturer's instructions. For gel electrophoresis, lysates containing 45  $\mu\text{g}$  of protein per lane were loaded onto a 5% stacking gel and 8% or 10% SDS-polyacrylamide separating gel. Electrophoretic transfer onto polyvinylidene difluoride (PVDF) membranes was carried out at 4 °C for 1.5 h at 150 V and 350 mA. Subsequently,

membranes were blocked with 5% fat-free milk for 1 h at room temperature. Primary antibodies (see Table 2) were then incubated with the membranes at 4 °C for a minimum of 8 h. Afterward, membranes were rinsed with tris-buffered saline containing 0.1% tween-20 (TBS-t) to remove residual unconjugated antibodies. Membranes were further probed with secondary antibodies conjugated to HRP enzyme for 1 h at room temperature. Image acquisition was performed using a Luminescence Imaging system (GE Amersham Imager 600, Waltham, USA) after additional washing with TBS-t and incubation with the enhanced chemiluminescence (ECL) substrates (Merck Millipore, Burlington, MA, USA). We utilized ImageJ for quantifying signal intensity, adjusting the values relative to the loading control for comparison.

### Statistical analysis

Animals were randomly assigned to each group, with sample sizes closely aligning with those reported in our previous studies [31–33, 36]. Statistical analysis was conducted in a blinded manner using GraphPad Prism software (version 7, GraphPad Software Inc., San Diego, CA, USA). Data are presented as mean  $\pm$  standard deviation (SD) or standard error of the mean (SEM), as specified in the figure legends. For datasets that passed the Shapiro-Wilk test for normality, one-way analysis of variance (ANOVA) followed by post-hoc tests, as indicated in the figure legends, were used to compare multiple groups. For datasets failing the normality test, Mann-Whitney U-tests and Kruskal-Wallis tests with post-hoc Dunn's test were applied. A significance level of  $p < 0.05$  was considered statistically significant.

## Results

### Neuronal TRPM8 exhibited a homogeneous distribution throughout the cerebral cortex

In this study, we first mapped the distribution of TRPM8 in the cerebral cortex of rats. The protein level of TRPM8 remained consistent across rostral (+2 to 0 mm), medial (0 to -2 mm), and caudal (-2 to -4 mm) sections (Fig. 1A). Notably, TRPM8 exhibited a homogeneous and diffuse expression pattern throughout the superficial cortical layers (layers II–III) across the rostral, medial, and caudal regions of the cerebral cortex (Fig. 1B). Subregional analysis also revealed a uniform expression pattern of TRPM8 among the dorsal, lateral, and ventral areas (Additional file 1), where TRPM8-expressing neurons accounted for 66.2–84.5% of all neurons. Furthermore, 80.6–94.1% of TRPM8+ cells were identified as neurons (Additional file 1B-1C). These observations were corroborated by Western blotting results, indicating a consistent distribution of TRPM8-expressing cells in the cortex. To further characterize the types of cells expressing TRPM8, immunofluorescence was conducted. Clearly defined fluorescence

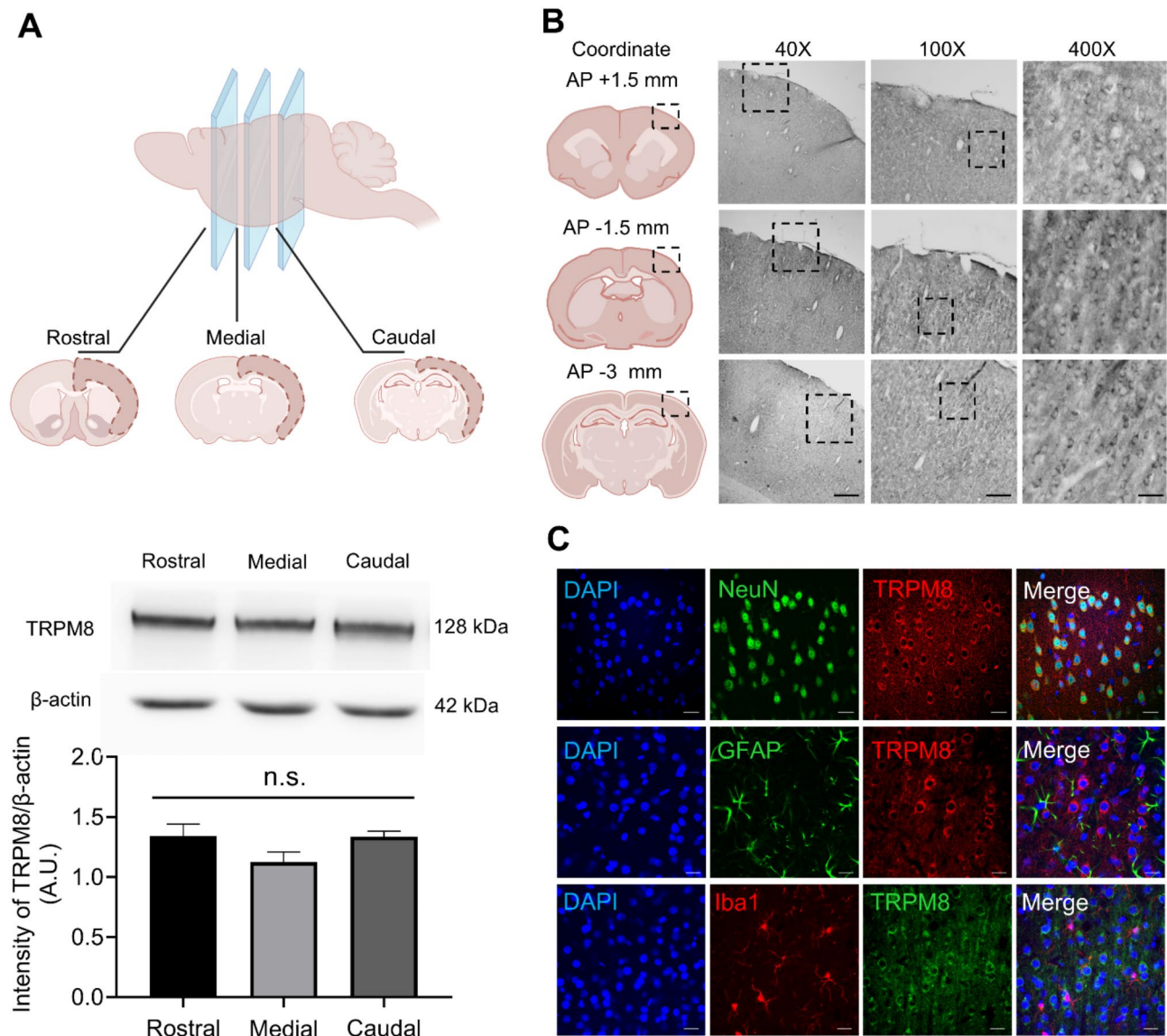


**Fig. 1** Uniform distribution of neuronal TRPM8 across the cerebral cortex. **(A)** Western blot analysis indicates consistent protein levels of TRPM8 across rostral (+2 to 0 mm), median (0 to -2 mm), and caudal (-2 to -4 mm) sections.  $n=3$ . **(B)** Immunohistochemistry demonstrates a homogeneous and diffuse expression pattern of TRPM8 throughout layers II~III of the cerebral cortex at AP +1.5, AP -1.5, and AP -3 mm. Images are shown at magnifications of 40X, 100X, and 400X. Scale bars represent 500  $\mu$ m, 125  $\mu$ m, and 50  $\mu$ m for 40X, 100X, and 400X magnifications, respectively. **(C)** Immunofluorescence staining demonstrates colocalization of TRPM8 with NeuN (neuronal marker) and minimal to no colocalization with GFAP (astroglial marker) and Iba1 (microglial marker). Scale bar = 20  $\mu$ m

signals were observed in cortical neurons, while neither microglia nor astrocytes exhibited TRPM8 expression (Fig. 1C).

#### Activation of cerebral TRPM8 enhances susceptibility to SD

To investigate the central effects of TRPM8 on migraine pathogenesis, we assessed the impact of TRPM8 on susceptibility to SD. We analyzed the frequency, duration, and amplitude of SD following the central administration of a TRPM8 agonist via two distinct routes. Icilin, a synthetic TRPM8 agonist, was i.c.v. injected prior to

SD induction. Our results revealed icilin (50–500  $\mu$ M) increased the frequency of KCl-induced SD (Fig. 2B). To assess the endogenous role of TRPM8 in SD susceptibility, we administered the TRPM8 antagonist M8-B via i.c.v. injection and topical application to the cerebral cortex. Interestingly, neither i.c.v. injection (5–50  $\mu$ M) nor topical application of M8-B (50  $\mu$ M) altered the frequency of SDs (Fig. 2C). TRPM8 activity modulation via i.c.v. injection did not influence the amplitude and duration of SD, except for a significant difference observed

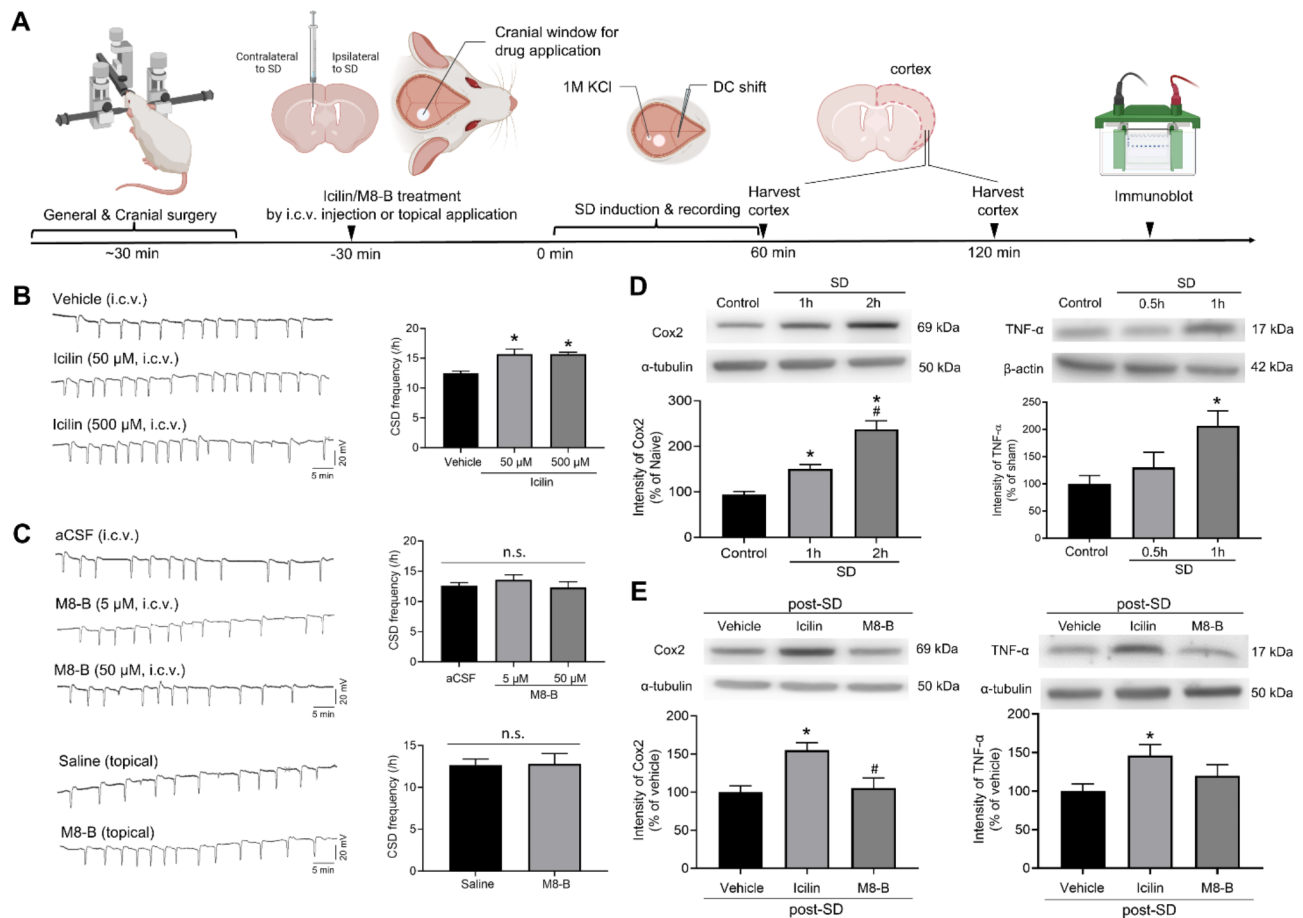


**Fig. 2** Effect of cerebral TRPM8 activation and inhibition on susceptibility to SD and SD-induced cortical inflammation. **(A)** Experimental timeline. **(B)** Effects of cerebral TRPM8 activation by icilin (50–500 μM) on KCl-induced SD frequency compared to the vehicle group (1% DMSO in aCSF). Data include  $n = 6$  for the vehicle and icilin 50 μM groups, and  $n = 3$  for the icilin 500 μM group. Statistical significance was observed ( $*p = 0.0153$  for the icilin 50 μM group versus vehicle,  $*p = 0.0393$  for the icilin 500 μM group versus vehicle; Kruskal-Wallis test). **(C)** Effects of cortical TRPM8 inhibition via i.c.v. injection or topical application of the TRPM8 antagonist M8-B (5 or 50 μM) on KCl-induced SD frequency. For the i.c.v. group,  $n = 5$  for vehicle and  $n = 7$  for M8-B ( $p = 0.6654$ , one-way ANOVA); for the topical group,  $n = 6$  for vehicle and  $n = 5$  for M8-B ( $p = 0.9247$ , unpaired t-test). **(D)** Western blot analysis showing temporal changes in SD-induced upregulation of Cox2 and TNF-α protein expression in the cerebral cortex. For Cox2,  $n = 4$  per group, with  $*p = 0.0288$  for the SD 1 h group versus control,  $p < 0.0001$  for the SD 2 h group versus control, and  $\#p = 0.0024$  for SD 1 h versus SD 2 h. For TNF-α,  $n = 4$  for control and post-SD 0.5 h groups, and  $n = 6$  for the post-SD 1 h group, with  $*p = 0.0166$  for the post-SD 1 h group versus control (one-way ANOVA followed by Tukey's post hoc test). **(E)** Effects of TRPM8 activation or inhibition by i.c.v. injection of icilin or M8-B on SD-induced Cox2 expression compared to the vehicle control. For Cox2,  $n = 4$  per group with  $*p = 0.0121$  versus vehicle,  $\#p = 0.0209$  versus icilin. For TNF-α,  $n = 8$  per group with  $*p = 0.0408$  versus vehicle (one-way ANOVA followed by Tukey's post hoc test). Data are presented as mean ± SEM

between the M8-B topical group and the saline topical group (Table 3).

SD-induced cortical neuroinflammation plays a critical role in headache initiation and persistence [36, 39]. SD upregulated the inflammatory markers cyclooxygenase 2 (Cox2) and tumor necrosis factor-α (TNF-α) 1 h after SD induction (Fig. 2D), consistent with previous findings [36, 39, 40]. This effect was further enhanced by TRPM8 activation using icilin (Fig. 2E). However, TRPM8 inhibition using M8-B did not significantly alter SD-induced Cox2 and TNF-α expression (Fig. 2E), consistent with the observed SD frequency (Fig. 2C). Icilin caused a slight increase in pro-CGRP expression levels, while M8-B had no significant effect on cortical pro-CGRP expression

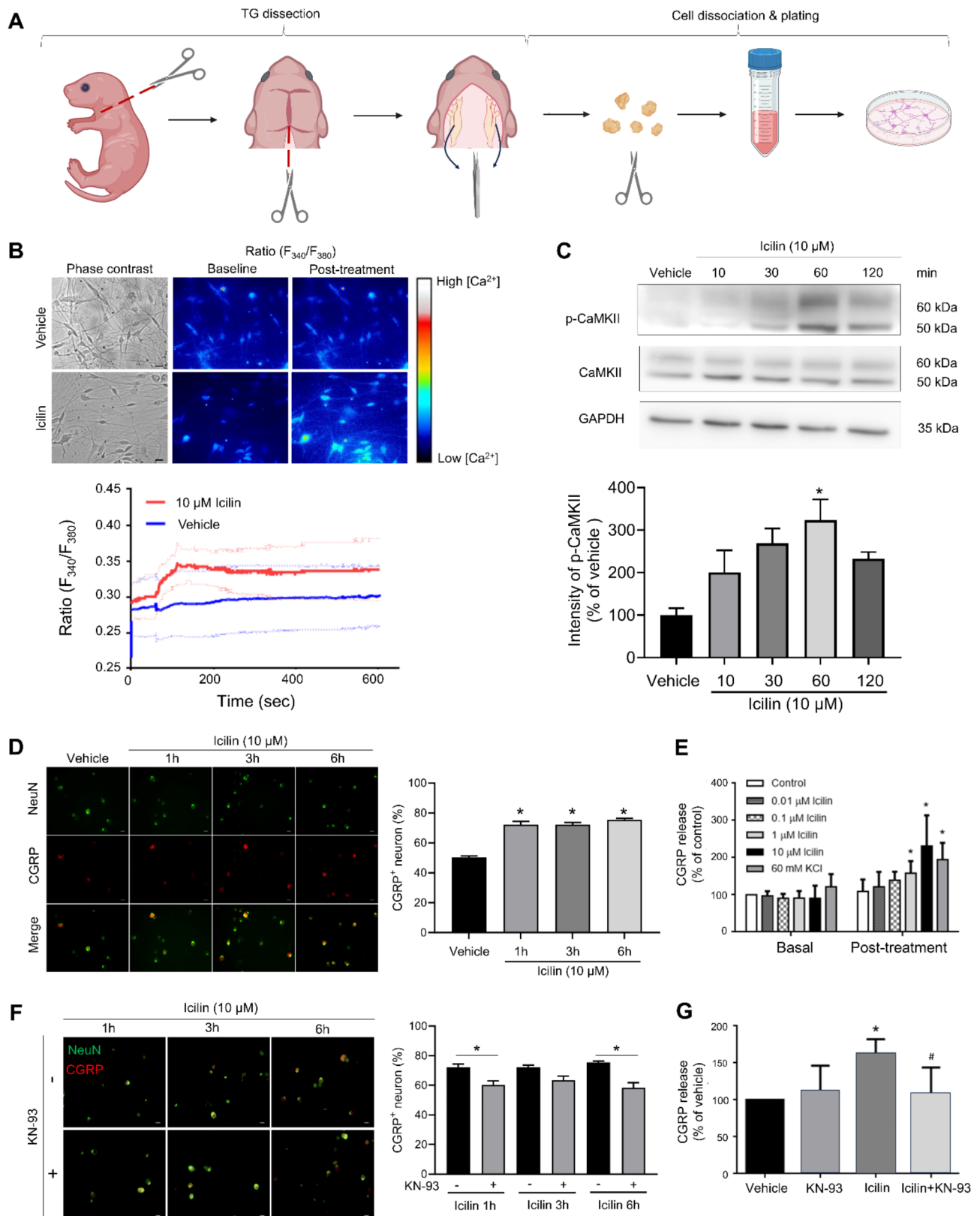


**Fig. 3** (See legend on next page.)

(See figure on previous page.)

**Fig. 3** Activation of TRPM8 induced CGRP upregulation and release in primary TG cells via CaMKII-dependent mechanism. **(A)** Schematic diagram illustrating the procedure for primary cultures of TG cells derived from postnatal day 8 to day 10 rats. **(B)** Effects of icilin on intracellular  $\text{Ca}^{2+}$  dynamics in vehicle- and icilin-treated cultured cells. Upper panel: Representative images of intracellular  $\text{Ca}^{2+}$  dynamics in vehicle- and icilin-treated groups. The left panel shows phase contrast images of cultured cells in both groups (scale bar = 20  $\mu\text{m}$ ). The middle and right panels show pseudocolor representations of F340 nm/F380 nm ratios before and after treatment, respectively. Lower panel: temporal changes in intracellular calcium concentration following TRPM8 agonist icilin (10  $\mu\text{M}$ ) treatment, represented as the mean ratio of 340 nm ( $\text{Ca}^{2+}$ -bound Fura-2) to 380 nm ( $\text{Ca}^{2+}$ -unbound Fura-2) fluorescence signals in vehicle (blue line) and icilin-treated (red line) groups. For the vehicle group, data were obtained from the TG of 8 rats, with tissues pooled from 4 animals and cultured in two separate dishes. For the icilin group, data were obtained from the TG of 5 rats, with tissues pooled from 2 animals for one culture dish and from 3 animals for another culture dish. Fura-2 was loaded into the cells in each dish for calcium ion signaling detection. The shaded plots represent individual data sets showing temporal changes in  $\text{Ca}^{2+}$  signaling for both the vehicle (blue line) and icilin (red line) groups. The bold line represents the average of the two individual culture data sets. **(C)** Western blot analysis showing the temporal changes in TRPM8 activation and its effect on phosphorylated CaMKII expression ( $n=3$ ;  $*p=0.011$  versus control group, one-way ANOVA followed by Tukey's post-hoc test). **(D)** Immunofluorescence staining demonstrates the expression of CGRP following icilin (10  $\mu\text{M}$ ) treatment compared to the vehicle group ( $n=3$ ;  $*p<0.0001$  versus vehicle group). **(E)** Effects of TRPM8 activation on extracellular CGRP levels in the culture medium, with KCl (60 mM) serving as a positive control ( $n=3$ ;  $*p=0.02$ , 0.0001, and 0.002 for icilin at 1  $\mu\text{M}$ , 10  $\mu\text{M}$ , and KCl, respectively, versus their basal levels). **(F)** The effects of pretreatment with the CaMKII inhibitor KN-93 (5  $\mu\text{M}$ , 10-minute pretreatment) on icilin-induced CGRP upregulation ( $n=3$ ;  $*p<0.0001$  versus vehicle group;  $\#p=0.026$  for vehicle vs. icilin at 1 h,  $\#p=0.0009$  for vehicle vs. icilin at 6 h, two-way ANOVA). **(G)** The effects of CaMKII inhibition by KN-93 (5  $\mu\text{M}$ ) on icilin-induced extracellular CGRP levels following icilin treatment ( $n=3$ ;  $*p=0.01$  versus vehicle group;  $\#p=0.03$  vs. icilin group, one-way ANOVA). Immunofluorescence staining and western blot data are presented as mean  $\pm$  SEM. CGRP release data are expressed as mean  $\pm$  SD. Scale bar: 20  $\mu\text{m}$

(Additional file 2 A). Additionally, TRPM8 expression decreased following 2 h of SD induction (Additional file 2B) but remained stable when pretreated with icilin or M8-B (Additional file 2C) or when these treatments were combined with SD (Additional file 2D). In summary, our findings suggest that cerebral TRPM8 activation increases both SD frequency and SD-induced cortical inflammation, while TRPM8 inhibition does not significantly affect KCl-evoked SD or SD-induced cortical inflammation. From the perspective of TRPM8's central role, TRPM8 activity may contribute to increased susceptibility to migraine.

#### Activation of TRPM8 in the TG induces the upregulation and release of CGRP through CaMKII-dependent mechanism

To elucidate the peripheral role of TRPM8 in migraine pathogenesis, we utilized primary cultures of TG cells derived from postnatal day 8 to day 10 rats, selected for their higher cell yield compared to adult rats (Fig. 3A, Additional file 3A). Differential interference contrast (DIC) imaging demonstrated that neurons cultured for 8 days in vitro (DIV8) exhibited significantly higher adhesion rates and a more mature morphology, characterized by well-developed neuronal processes, compared to neurons at earlier stages of differentiation (Additional file 3B). Consequently, DIV8 neurons were chosen for subsequent experimental treatments. In these primary TG cultures, neurons constituted 50.88% of all cells, with 52.31% of these expressing TRPM8. Additionally, 50.01% of the cells were identified as CGRP-positive neurons (Additional file 3 C-E).

TRPM8, a non-selective cation channel, facilitates  $\text{Ca}^{2+}$  influx into the cell upon activation. We assessed intracellular calcium levels following TRPM8 activation using the calcium indicator Fura-2. In the vehicle group,  $11.5 \pm 5.4\%$  of cells exhibited a slight increase in intracellular  $\text{Ca}^{2+}$

concentration, reflecting basal  $\text{Ca}^{2+}$  dynamics over time. In contrast,  $59.2 \pm 5.4\%$  of cells in the icilin-treated group showed a rapid 13% increase in intracellular calcium levels within 2 min, with this elevation sustained for at least 10 min (Fig. 3B). This response aligns with our result that approximately 50% of the cells express TRPM8 (Additional file 3C), suggesting that most TRPM8-positive cells respond to icilin stimulation (Fig. 3B). Furthermore, icilin triggered a time-dependent activation of calmodulin kinase II (CaMKII), a crucial downstream signaling molecule for  $\text{Ca}^{2+}$ , with peak activation observed at 1 h and a subsequent decline at 2 h (Fig. 3C). To investigate the effects of TRPM8 activation on the expression and release of CGRP in primary TG cells, we performed immunofluorescence staining. This revealed a significant increase in neuronal CGRP levels following icilin treatment compared to the vehicle group (Fig. 3D). We also measured extracellular CGRP levels in the medium to evaluate CGRP release. As the spontaneous release of CGRP by the cells in the absence of exogenous stimuli could not be confirmed, measuring the CGRP concentration in the medium alone would make it difficult to discern whether the observed response was due to drug treatment or intrinsic cellular release. Therefore, we utilized 60 mM KCl in the CGRP release experiments as a positive control for external stimuli-induced CGRP release, based on prior studies demonstrating that KCl stimulates CGRP release [41]. Our results demonstrated that icilin promoted CGRP release in a dose-dependent manner (Fig. 3E). To determine whether TRPM8-induced CGRP upregulation and release occurs via the CaMKII pathway, we utilized the CaMKII inhibitor KN-93. Pretreatment with KN-93 attenuated icilin-induced CGRP upregulation (Fig. 3F) and inhibited icilin-induced CGRP release (Fig. 3G). Additionally, we explored the role of extracellular  $\text{Ca}^{2+}$  in icilin-induced CGRP release by employing a  $\text{Ca}^{2+}$ -free medium supplemented with the chelating agent

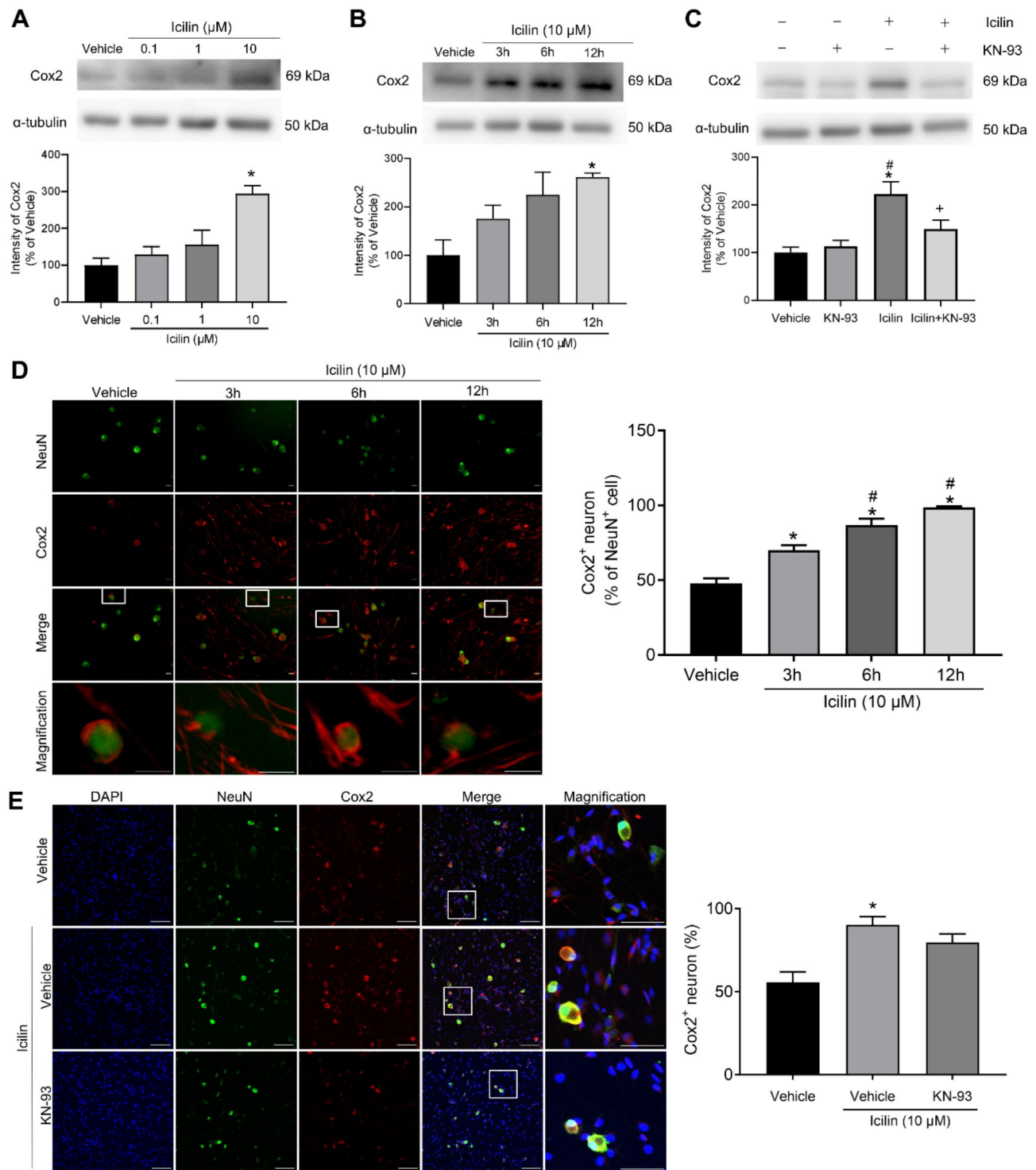


**Fig. 4** (See legend on next page.)

BAPTA (Additional file 4 A). The absence of extracellular Ca<sup>2+</sup> significantly reduced icilin-induced CGRP release (Additional file 4B), indicating that icilin facilitates CGRP release through a mechanism dependent on extracellular Ca<sup>2+</sup> influx. In summary, our findings suggest that

TRPM8 activation in trigeminal neurons upregulates CGRP and promotes its release via a Ca<sup>2+</sup>/CaMKII-dependent mechanism.

(See figure on previous page.)

**Fig. 4** Activation of TRPM8 in primary TG cells induced neuroinflammation via CaMKII-dependent mechanism. **(A)** Effects of icilin treatment on Cox2 expression in primary TG cells ( $n=5$ ;  $*p=0.0139$  vs. vehicle control, Kruskal-Wallis test followed by Dunn's post-hoc analysis). **(B)** Temporal dynamics of icilin-induced Cox2 expression ( $n=4$ ;  $*p=0.0162$  vs. vehicle control, one-way ANOVA followed by Tukey's post-hoc test). **(C)** Western blot analysis showing the effect of CaMKII inhibition by KN-93 (5  $\mu\text{M}$ ) on icilin-induced Cox2 upregulation ( $n=5$ ;  $*p=0.0012$  vs. vehicle control,  $\#p=0.0028$  vs. KN-93 group,  $+p=0.0445$  vs. icilin group, one-way ANOVA followed by Holm-Sidak's post-hoc analysis). **(D)** Immunofluorescence staining demonstrates icilin-induced Cox2 expression (red fluorescence) co-localized with NeuN, a neuronal marker (green fluorescence) in TG cells. Scale bar = 20  $\mu\text{m}$ . Quantitative analysis shows the percentage of Cox2+ neurons ( $n=3$ ;  $*p=0.0051, 0.0001, \text{ and } <0.0001$  for icilin at 3 h, 6 h, and 12 h, respectively, vs. vehicle group;  $\#p=0.0271$  for icilin at 6 h and  $p=0.0011$  for icilin at 12 h vs. icilin at 3 h, one-way ANOVA). **(E)** Immunofluorescence staining illustrates the effects of KN-93 inhibition on icilin-induced Cox2 expression in TG neurons. Scale bar = 100  $\mu\text{m}$ . White boxes indicate the regions that are shown at higher magnification in the adjacent panels, providing a clearer view of Cox-2 localization. Scale bar in the magnified images = 50  $\mu\text{m}$ . Quantitative results indicate the percentage of Cox2+ neurons ( $n=3$ ;  $*p=0.0219$  vs. vehicle group, Kruskal-Wallis test). Data are presented as mean  $\pm$  SEM

### Activation of trigeminal TRPM8 induces CaMKII-dependent neuroinflammation

Finally, we investigated the impact of TRPM8 on neuroinflammation. Treatment with icilin resulted in a dose- and time-dependent increase in Cox2 levels, observed at 12 h (Fig. 4A-B). Inhibition of CaMKII with KN-93 did not significantly alter the basal expression of Cox2. However, KN-93 pretreatment effectively attenuated icilin-induced Cox2 upregulation (Fig. 4C). Immunofluorescence staining confirmed that Cox2-expressing cells were predominantly trigeminal neurons, as evidenced by their co-localization with NeuN-positive neurons (Fig. 4D). Moreover, icilin-evoked Cox2 expression was reduced by CaMKII inhibition, underscoring the role of CaMKII in mediating neuroinflammation downstream of TRPM8 (Fig. 4E). Additionally, we examined the role of CGRP in icilin-induced trigeminal neuroinflammation using BIBN4096, a CGRP receptor antagonist. Immunostaining revealed that icilin-induced Cox2 expression was attenuated by co-treatment with BIBN4096 at 3 and 6 h (Additional file 5 A-B). Western blot analysis further confirmed that icilin-induced Cox2 upregulation was significantly reduced in cells co-treated with a high concentration (10  $\mu\text{M}$ ) of BIBN4096 (Additional file 5 C). In summary, our findings indicate that activation of peripheral TRPM8, particularly within the trigeminal ganglion, plays a significant role in driving trigeminal neuroinflammation.

### Discussion

This study provides novel insights into the potential role of TRPM8 in migraine by exploring its central effects on SD and its peripheral effects on TG neuronal activity and inflammation. By demonstrating that activation of cortical neuronal TRPM8 increases susceptibility to SD and SD-evoked cortical neuroinflammation, possibly independent of intrinsic regulatory mechanisms, our findings shed light on previously unexplored central aspects of cortical TRPM8 function. Furthermore, our results also address the peripheral contribution, specifically, trigeminal TRPM8 activation, to the release and expression of CGRP and trigeminal neuroinflammatory responses via a CaMKII-dependent mechanism.

Collectively, these findings underscore the central and peripheral TRPM8 functions, providing insights into possible therapeutic strategies targeting TRPM8 for migraine.

### Potential mechanisms underlying TRPM8's influence on SD, TG neuron, and migraine-related behaviors

To the best of our knowledge, this study is among the first to explore the potential relationship between TRPM8 and cortical SD (Fig. 2B and C). Our findings suggest that TRPM8 activation may increase the frequency of SD events. Elevations in extracellular glutamate and  $\text{K}^+$  are crucial for initiating and propagation of SD. It is plausible that TRPM8 activation influences SD susceptibility by increasing intracellular  $\text{Ca}^{2+}$  levels, which could contribute to neurotransmitter release. Studies indicate that menthol-induced TRPM8 activation leads to glutamate release from DRG neuronal terminals [42–44]. Furthermore, TRPM8 has been reported to activate large-conductance  $\text{Ca}^{2+}$ -activated  $\text{K}^+$  channels (BK channels), promoting the outward  $\text{K}^+$  flow upon  $\text{Ca}^{2+}$  influx [45]. Notably, TRPM8 activation has been linked to increased neuronal excitability by inhibiting leak  $\text{K}^+$  conductance [46], potentially accounting for the depolarized resting membrane potential observed after SD. These findings suggest that TRPM8 activity may modulate susceptibility to SD by affecting excitatory neurotransmission,  $\text{K}^+$  efflux, and intrinsic neuronal membrane properties.

The propagation of SD is critically dependent on  $\text{Ca}^{2+}$  influx. Previous studies have shown that SD triggered by localized high  $\text{K}^+$  or brief electrical stimulation requires  $\text{Ca}^{2+}$  for its propagation [47, 48]. For example, in rat neocortical slices, pre-treatment with  $\text{Ca}^{2+}$ -free media completely prevented SD induced by localized high  $\text{K}^+$  exposure [49]. Similarly, non-selective  $\text{Ca}^{2+}$  channel blockers have been shown to prevent SD propagation in hippocampal slices following high  $\text{K}^+$  exposure, further supporting the notion that calcium influx is essential for SD spread [50]. Studies in genetically modified mice with mutations in the P/Q-type  $\text{Ca}^{2+}$  channel gene (CACN1A) provide additional evidence for the crucial role of calcium in SD propagation [51–53]. Gain-of-function knock-in mutations of the *Cacna1a* gene have been associated

with reduced SD thresholds and accelerated propagation speed, underscoring the potential involvement of P/Q-type channels in SD regulation. Since P/Q-type  $\text{Ca}^{2+}$  channels mediate calcium-dependent neurotransmitter release [52], both non-selective  $\text{Ca}^{2+}$  channel blockers and selective inhibitors of P/Q-type channels effectively block SD propagation [53], further emphasizing the essential role of  $\text{Ca}^{2+}$  influx in SD propagation.

CaMKII, a serine/threonine kinase, is activated in response to elevated intracellular  $\text{Ca}^{2+}$  levels [54]. In our TG primary culture experiments, we observed that TRPM8 activation leads to CaMKII activation (Fig. 3C). While this mechanism has not been directly examined in the cerebral cortex, it is reasonable to hypothesize that TRPM8 in the cortex may operate through pathways similar to those identified in the TG. Although direct evidence linking CaMKII to SD susceptibility is lacking, previous studies have reported that SD triggers transient and reversible widespread fission of the cortical endoplasmic reticulum (ER). Furthermore, CaMKII inhibition has been shown to mitigate SD-induced neuronal activity suppression and prevent ER fission [55]. TRPM8 activation may elevate intracellular  $\text{Ca}^{2+}$  levels, which may potentially initiate downstream signaling events such as CaMKII activation. We speculate that this cascade could play a role in SD-related events, such as CaMKII-mediated ER fission and associated neuronal dysfunction.

Previous studies have explored the potential role of TRPM8 in pain or migraine-related behaviors, including the mechanical allodynia in nitroglycerin (NTG)-induced chronic migraine model, but the results have been inconsistent, likely influenced by various factors. The function of TRPM8 appears to depend on the context of injury. Under cold stimuli, TRPM8 mediates cold allodynia by regulating neuronal activity [43, 45, 46]. However, when exposed to stronger noxious stimuli, such as formalin or inflammatory soup, TRPM8 exhibits anti-nociceptive effects [23, 44]. In the NTG-induced chronic migraine model, conflicting results have also been observed. TRPM8 lowers the mechanical allodynia threshold during the NTG administration phase [18] but facilitates the recovery of allodynia thresholds following repeated NTG injections [24]. These findings suggest that TRPM8 may contribute to mechanical hypersensitivity in the presence of noxious stimuli. However, in the absence of noxious stimuli, TRPM8 plays a protective role in promoting recovery from hypersensitivity through endogenous testosterone, an endogenous ligand of TRPM8 [24]. Taken together with the effects observed in other animal models, we speculate that the role of TRPM8 in migraine-related mechanisms is not limited to a single pathway but likely involves contributions at multiple mechanisms, including modulating SD and nociceptive mechanisms.

TVS activation is pivotal in migraine pathogenesis. While the precise mechanism underlying TVS activation remains incompletely elucidated, meningeal vasodilation response, meningeal inflammation, and sensitization of TNC neurons are critical components of TVS activation. A study using intravital microscopy showed that TRPM8 activation by menthol altered the basal meningeal arterial tone, causing meningeal vasodilation [56]. In an ex vivo hemiskull model, menthol stimulated CGRP release from the hemiskull, TG, and TNC [57]. Furthermore, electrophysiological recordings demonstrate that menthol increased both excitatory and inhibitory synaptic transmission in the TCC [56, 58]. These findings raise a possibility that potential pronociceptive role of TRPM8.

#### Characterization of TRPM8 expression and activity

In our experiments, to minimize non-specific TRPM8 signals, we utilized a TRPM8 primary antibody that has been validated for specificity in knockout cells [63]. Our results show that the TRPM8 signal in TG cultures appeared relatively faint compared to markers such as beta III tubulin (Additional file 3D), likely reflecting the low endogenous expression of TRPM8 in these neurons under our experimental conditions. Our quantitative results revealed that approximately 50% of the culture consisted of neurons (Additional file 3 C), with around half of these neurons expressing TRPM8 (Additional file 3D), suggesting that TRPM8-positive cells accounted for roughly 25% of the total TG cell population. In contrast, previous studies using immunohistochemistry and in situ hybridization in rats and mice reported that TRPM8 is expressed in 11.8% of adult TG neurons [59] and 5–10% in adult DRG neurons [60], slightly lower than our finding (Additional file 3 C-D). The observed difference may be attributed to variations in experimental methodologies—ours is based on primary cultures, whereas previous studies typically employed tissue immunohistochemistry. Additionally, developmental dynamics of TRPM8 expression likely contribute to this discrepancy. TRPM8 expression follows a biphasic pattern during development [61]. It begins at E14 and increases significantly from E14 to E18 [61, 62], peaks at birth, and then declines by P4. A second wave of upregulation occurs between P4 and P12, followed by a slight reduction and eventual stabilization in adulthood [61]. The higher percentage of TRPM8-positive neurons observed in our primary cultures—around 25%, compared to approximately 5–11% in the literature—may stem from the fact that our cultures were derived from P8-P10 rat pups, which corresponds to the second developmental wave of TRPM8 upregulation. In contrast, several studies use adult rats, where TRPM8 expression in both the TG (the location of cell bodies of primary afferent neurons) and the

afferent fibers projecting to the meninges typically shows a decline compared to earlier developmental stages [9, 61].

The subcellular localization of TRPM8 was clarified by examining its distribution in relation to the cytoskeletal marker beta III tubulin. In the overlay images, circular hollow regions devoid of beta III tubulin staining correspond to the nuclei of the cells (Additional file 3D), as confirmed in a recent published study regarding TG primary culture [63]. The absence of TRPM8 signal in these nuclear regions indicates that TRPM8 does not localize to the nucleus, consistent with findings from recent studies [59]. A comparison of the single-channel TRPM8 staining image with the overlay image of beta III tubulin further supports the conclusion that TRPM8 is localized in the cytoplasm rather than the nuclear region.

Additionally, our TRPM8 staining in TG primary cultures exhibited a relatively uniform expression pattern, which may be attributed to the controlled cell seeding protocol used. Uneven seeding can result in variability in cell behavior, including differences in cell proliferation, differentiation, and cell-cell communication [64–66]. Maintaining consistent seeding density is crucial for obtaining reliable results, particularly in biomolecular assays, such as those analyzing supernatants and components isolated from cell lysates [67, 68]. However, while our primary cultures exhibit a relatively uniform TRPM8 expression pattern, this may not fully reflect the *in vivo* distribution of TRPM8 in TG tissue. In tissue sections, TG cells typically exhibit an uneven distribution, as demonstrated in previous studies [33, 36, 59]. The uniform distribution of TRPM8 in our primary cultures may be a consequence of the controlled seeding process, which contrasts with the more heterogeneous expression pattern seen in tissue. Therefore, the TRPM8 distribution in our cultured TG neurons may not directly mirror the expression pattern in intact TG tissue. Regarding TRPM8 expression, most studies have focused on its presence in the peripheral nervous system, including TG and DRG [59]. To the best of our knowledge, TRPM8 expression in the brain has primarily been documented using techniques such as western blot [10] or *in situ* hybridization [11]. Here, we provide the first evidence of TRPM8 protein expression in the cerebral cortex, highlighting its spatial distribution. TRPM8 is extensively expressed in cortical neurons, accounting for 66.2–84.5% of the neuronal population (Fig. 1 & Additional file 1), which is notably higher than the expression levels observed in TG primary neurons. TRPM8 expression in both the cortex and TG is primarily localized to neurons. Despite this similarity, the distribution of TRPM8 differs between the two tissues. In the cortex, TRPM8 is more uniformly expressed across cortical neurons, whereas in intact TG tissue, it shows a more uneven distribution. This

difference likely reflects the distinct spatial distribution pattern and neuronal organization in each tissue.

TRPM8 is a  $\text{Ca}^{2+}$ -permeable channel. In our study, we measured intracellular  $\text{Ca}^{2+}$  levels using the 340/380 nm excitation ratio for Fura-2 as an indicator of TRPM8 activation. Our results showed a modest increase in the ratio from 0.30 to 0.35, indicating a small change of 0.05 following icilin treatment. In contrast, a previous study using stable TRPM8-expressing cell lines reported a much larger  $\Delta 340/380$  change of approximately 3 to 4 at the same icilin concentration (10  $\mu\text{M}$ ) [69]. A significant challenge in our study was the limited cell yield from TG primary cultures, which required pooling cells for functional assays. Additionally, as noted earlier, the endogenous expression of TRPM8 in both TG primary cultures and intact TG tissue is low, which made  $\text{Ca}^{2+}$  level measurements particularly challenging. The TRPM8-expressing cell lines used in previous studies showed high TRPM8 expression (though the exact percentage was unspecified, images indicated a high proportion of transfected cells) [69], and our findings likely reflect the lower TRPM8 expression levels inherent to our experimental conditions. This difference may account for the relatively small response observed in our study.

Our findings show that after icilin treatment, the  $\text{Ca}^{2+}$  concentration rises and remains elevated above baseline for at least 500 s (Fig. 3B). However, these changes may not fully reflect calcium channel activity. A previous study demonstrated that while  $\text{Ca}^{2+}$  current changes return to baseline within approximately 5 s under continuous icilin exposure, intracellular  $\text{Ca}^{2+}$  concentrations remain elevated for up to 100 s [69]. Although the previous study did not assess longer-term changes in intracellular  $\text{Ca}^{2+}$  levels (i.e., beyond 100 s), their results, showing no noticeable recovery in  $\text{Ca}^{2+}$  concentration, are consistent with our findings (Fig. 3B). This suggests that intracellular  $\text{Ca}^{2+}$  dynamics may not entirely capture the transient nature of  $\text{Ca}^{2+}$  currents.  $\text{Ca}^{2+}$  currents, driven by the rapid movement of ions across the membrane, are tightly regulated by membrane potential and typically last milliseconds to seconds. In contrast, intracellular  $\text{Ca}^{2+}$  dynamics involve more complex processes, such as  $\text{Ca}^{2+}$  entry, release from intracellular stores, buffering by cytosolic proteins, and diffusion, which sustain changes for tens to hundreds of seconds [70], which contribute to sustained changes lasting tens to hundreds of seconds. Importantly, these sustained changes do not necessarily diminish the functional relevance of the initial  $\text{Ca}^{2+}$  rise above baseline observed after icilin treatment (Fig. 3B). On the contrary, they highlight the complexity of evaluating  $\text{Ca}^{2+}$  channel activity based solely on intracellular  $\text{Ca}^{2+}$  levels. The duration of the elevated  $\text{Ca}^{2+}$  state may be influenced by buffering mechanisms or the diffusion rate of  $\text{Ca}^{2+}$  indicators, which could limit its ability

to fully reflect ion channel activity compared to current recordings. Therefore, the prolonged intracellular  $\text{Ca}^{2+}$  responses are likely driven by downstream processes, rather than continuous TRPM8 activity, indicating a limitation of the calcium imaging technique. Nonetheless, these prolonged responses do not negate the physiological significance of the initial  $\text{Ca}^{2+}$  rise induced by icilin.

#### **Possible mechanisms regulating TRPM8 expression and activity**

We present novel evidence demonstrating that TRPM8 exhibits a nearly homogeneous distribution in the cerebral cortex (Additional file 1) and demonstrate that SD downregulates TRPM8 expression (Additional file 2B). TRPM8 expression or activity is modulated by several molecules, including PIP2 [71] and protein kinase C (PKC) [72–74]. SD has been reported to enhance PKC activity in the cerebral cortex [75] and PKC-mediated desensitization of TRPM8 has been documented [72–74]. Therefore, SD-induced PKC activation may plausibly contribute to the observed reduction in TRPM8 expression following SD. Additionally, F11, a TRPM8 agonist, has been shown to increase TRPM8 expression on the plasma membrane [76], which could potentially rescue TRPM8 expression following SD induction, and might explain why TRPM8 expression remained unchanged when icilin treatment was followed by SD induction (Additional file 2D). The lack of significant changes in TRPM8 expression after icilin treatment alone (Additional file 2C) may be attributed to this transient, agonist-dependent recruitment of TRPM8. From a pathophysiological perspective, our findings suggest that while TRPM8 may facilitate susceptibility to SD, the SD-induced downregulation of TRPM8 could serve as a compensatory mechanism to mitigate the effects of TRPM8 activation. Currently, there is a lack of literature explaining why TRPM8 expression is downregulated after SD induction. However, based on our findings suggesting a potential compensatory mechanism, future experiments could aim to investigate this further. One approach could involve utilizing optogenetic techniques to induce repeated SD events in awake animals. This method would allow the assessment of SD susceptibility at multiple time points after the initial induction, including 2 h or longer. By performing repeated SD inductions in awake animals, it could be determined whether the observed downregulation of TRPM8 leads to reduced susceptibility to SD in subsequent tests, which would help clarify the role of TRPM8 in modulating SD.

GWAS have identified a significant association between specific SNPs within the TRPM8 gene, specifically rs10166942[C/T] and rs17862920[T/C], and an increased susceptibility to migraine. Importantly, analysis of TRPM8 mRNA expression in the DRG has revealed

lower expression level associated with the chromosome harboring rs10166942[C], in contrast to the chromosome carrying the rs10166942[T] variant [6]. Individuals bearing C-allele in the rs10166942 variant exhibit a significantly reduced sensitivity to cold pain compared to non C-allele carriers [6], while those the rs10166942[T] allele exhibit an increased risk of migraine [3–5]. Moreover, migraine patients with the rs10166942[T] allele are predisposed to chronic migraine and allodynic symptoms [5]. This observed association suggests that genetic polymorphisms could influence TRPM8 expression and activity, and potentially contributing to an increased susceptibility to migraine.

#### **TRPM8 and neuroinflammation**

Animal studies suggest that SD triggers the opening of pannexin 1 (PANX1), facilitating the formation of the  $\text{P2}\times\text{7}$ -PANX1 pore complex. This complex enables subsequent activation of the  $\text{P2}\times\text{7}$  receptor, which plays a crucial role in SD-induced neuroinflammation [36, 39, 77, 78]. Although there is no direct evidence explaining how TRPM8 activation by icilin treatment enhances SD-induced cortical neuron inflammation, purinergic  $\text{P2}\times\text{7}$ -mediated mechanisms may still be involved. TRPM8 activators have been shown to increase ATP release [79]. Additionally, inhibition of pannexin 1 suppresses TRPM8-induced ciliary beat frequency, suggesting that purinergic receptors might be part of the downstream signaling pathway activated by TRPM8 and could contribute to its effects.

Regarding the relationship between SD and TG inflammation, we previously examined Cox2 expression in the TG following SD, but found no significant change in Cox2 expression after CSD [33]. Given that SD induces CGRP upregulation and neuronal sensitization in the TG [64, 77], and considering that CGRP is known to trigger TG inflammation through activation of its receptor in satellite glial cells [80–82], we speculate that SD may induce TG inflammation through CGRP-related mechanisms. Previous studies have indicated that  $\text{P2}\times\text{7}$  inhibitors can reduce CGRP expression in the TG [77], suggesting that  $\text{P2}\times\text{7}$  may play a role in modulating TG inflammation, potentially through CGRP regulation. Although no direct evidence links  $\text{P2}\times\text{7}$  activation to Cox2 expression in the TG, it is possible that CGRP could contribute to TG inflammation. In this study, we lack direct evidence addressing the relationship between cortical TRPM8 activation and SD-induced TG inflammation. As discussed, our previous finding of no significant SD-induced Cox2 expression in the TG may be attributed to the insufficient timepoint at which the tissue was harvested [33]. Future studies could address this question by evaluating different sampling time points.

Satellite glial cells can be distinguished in our TG cultures. Based on our results, we observed that not all DAPI signals colocalize with NeuN, and some Cox2 signals were found without NeuN colocalization (Fig. 4D-E). This suggests the presence of satellite glial cells in the TG cultures. However, our staining results also indicate that CGRP, a key mediator in TG inflammatory responses, is predominantly expressed in neurons. Previous studies have shown that satellite glial cells in the TG express functional CGRP receptors, and activation of these CGRP receptors can trigger inflammatory responses in the TG [47]. In our TG primary cultures, treatment with BIBN4096, a CGRP receptor antagonist, was able to suppress the inflammatory response induced by icilin (Additional file 5), which agrees with previous findings. Therefore, based on our findings of CGRP release and BIBN4096 treatment in TG primary cultures, we hypothesize that TRPM8 activation may promote the release of CGRP from TG neurons, which then acts on satellite glial cells and induces inflammation in the non-neuronal TG cells (Fig. 4D-E). However, to confirm this hypothesis, conditional knockout models that ablate CGRP in TG neurons and CGRP receptor in the satellite glial cells would be required for further validation.

#### Potential endogenous ligands for TRPM8

The mechanism underlying TRPM8 activation by cold stimuli within the skull remains unclear, as body temperatures rarely reach the levels required to trigger TRPM8 activation. It is plausible that TRPM8 activation may be triggered through mechanisms independent of cold stimuli. Although our results showed no direct effect of endogenous TRPM8 activity on SD (Fig. 2C), it remains possible that endogenous ligands of TRPM8 may be elevated under pathological conditions, thereby potentially facilitating TRPM8-mediated effects. Proposed endogenous ligands for TRPM8 include Phosphatidylinositol-4,5-bisphosphate (PIP2) [83], the growth factor artemin [84], the hormone testosterone [85], and the membrane protein Pirt [86]. Notably, artemin has been implicated in migraine. While direct clinical evidence of elevated artemin levels in migraine patients is lacking, preclinical studies have investigated the potential role of artemin in migraine. In the NTG model, both mRNA and protein level of artemin were found to increase in the dura mater [86]. In primary cultured TG cells, artemin induced the upregulation of inducible nitric oxide synthase [87], an inflammatory marker, suggesting artemin facilitates trigeminal neuroinflammation. However, the direct association between these ligands and TRPM8 activation requires further investigation. Further research into artemin levels in migraine patients would help elucidate the potential role of the endogenous TRPM8 activity in migraine pathogenesis.

#### Study limitation

There are several limitations in our study. First, a notable concern is the specificity of pharmacological manipulation of TRPM8 activity using icilin and M8-B. Both menthol and icilin are widely used TRPM8 agonists, with icilin demonstrating relatively higher potency and efficacy compared to menthol and other newly developed agonists [88]. Structural studies of TRPM8 have identified key residues, such as Gly<sup>805</sup> in the S3 region [89] and Arg<sup>841</sup> in the S4 region [90], which mediate icilin binding and subsequent activation of TRPM8. These interactions, including hydrogen bonding and stabilization of 3<sub>10</sub>-helical conformation, enable that TRPM8 interact with icilin using Arg<sup>841</sup> and His<sup>844</sup> residues [90]. Behavioral studies using genetically modified mice further indicate that icilin-induced acute cold pain responses are mediated by TRPM8 rather than TRPA1, which is supported by reduced responses in TRPM8-deficient and TRPM8/TRPA1 double-knockout mice, but not in TRPA1-deficient mice [91]. The potency and specificity of M8-B to inhibit TRPM8 are also supported by in vitro studies and genetically modified mice [92]. However, icilin has also been shown to activate TRPA1 at concentrations exceeding 100  $\mu$ M [93, 94]. In our in vivo experiments, icilin was applied at 50  $\mu$ M and 500  $\mu$ M. We acknowledge the absence of direct evidence confirming TRPM8 activation under our icilin treatment. Based on the specificity-related references discussed above, we speculate that the observed effects at 50  $\mu$ M are likely mediated through TRPM8 activation, whereas the potential involvement of TRPA1 at 500  $\mu$ M cannot be entirely excluded. In our in vitro study, the effective dose of icilin was 10  $\mu$ M, which is a slight higher than that used in previous primary afferent electrophysiology study, but still notably lower than the concentration required to activate TRPA1 [44]. We observed that M8-B did not significantly alter CSD frequency or cortical inflammation, suggesting that TRPM8 may have a limited or context-dependent role in regulating SD. This observation raises the possibility that TRPM8's involvement in CSD susceptibility may be conditional, requiring additional activating factors or specific physiological contexts, such as the presence of specific ligands and Ca<sup>2+</sup>, or under specific pH value. pH is reported to regulate TRPM8 efficacy, latency to action, and temperature threshold [69]. To address this limitation and further clarify the specificity of icilin's effects, future studies could explore the use of additional TRPM8-specific antagonists, co-administration of icilin and antagonists, or genetic approaches such as TRPM8<sup>Cre</sup> mice [95] and selective TRPM8-neuron ablation method [18]. To specifically characterize TRPM8 expression, TRPM8-EGFP reporter mice is a useful tool for further investigation [7]. Although our results suggest that TRPM8 is expressed at relatively low levels in TG

neurons, the signal remains detectable and aligns with its known cytoplasmic localization. For future studies aimed at enhancing TRPM8 detection, we recommend using TRPM8-EGFP reporter mice, which would provide stronger fluorescence signals, facilitating clearer visualization of TRPM8 expression.

Secondly, in the current study on SD experiments, we assessed only a single DC potential shift, which primarily indicates depolarization. However, other important read-outs, such as SD threshold and SD propagation, were not evaluated. As the rate of CSD propagation is an important parameter for understanding the dynamics of SD, this limitation in the current study should be acknowledged. To more comprehensively assess the effect of TRPM8 on SD susceptibility, future studies should incorporate additional measures, including the evaluation of SD threshold and propagation rate. Additionally, our study did not analyze the potential contribution of sex to the effect of TRPM8 on SD susceptibility, despite the higher prevalence of migraine in females. A study has shown that TRPM3, another member of the TRP channel family, exhibits more pronounced nociceptive firing in female mice compared to males. This sex-specific activation of TRPM3 raises the question of whether a similar sexual dimorphism might influence TRPM8's role in SD susceptibility. It is known that testosterone, a potential endogenous ligand for TRPM8, has been shown to facilitate sexual dimorphism by expediting the recovery process in males from NTG-induced hypersensitivity [24]. Our results indicated that SD frequency in male rats, even with higher testosterone levels, seems impervious to endogenous regulatory mechanisms associated with TRPM8 (Fig. 2C). Notably, testosterone has been reported to suppress SD via the androgen receptor [96]. These findings suggest that the impact of testosterone-mediated TRPM8 activation on SD susceptibility may be minor. Nonetheless, the effect of sex differences and hormone levels on TRPM8 in SD or TG neuronal function requires further investigation. The issues concerning the potential endogenous ligands of TRPM8, including their origin, endogenous levels, and temporal dynamics, remain to be further studied. Grasping these factors will be essential for a more thorough understanding of TRPM8's involvement in the pathophysiology of migraine.

Thirdly, the number of TG primary cultured neurons available for each experiment is limited. We observe the overall response of the entire neuronal population, rather than recording from individual cells. To overcome the limitation of cell numbers, we pooled neurons from the TGs of multiple animals to ensure sufficient cell numbers for each experimental condition. Consequently, we focused on incorporating KCl as a positive control primarily in experiments assessing CGRP release from TG

neurons, which we considered a critical functional read-out. Given the limited availability of cells, we prioritized the inclusion of KCl in these experiments, while omitting it from other assays. Nevertheless, we recognize that co-administration of M8-B with icilin or KCl would have provided a more selective approach to assess the role of TRPM8 in evoked neuronal activity. Specifically, co-treatment with M8-B would enable us to better isolate the contribution of TRPM8 to KCl-induced responses and minimize the potential for non-specific effects associated with icilin. Although the limitations on cell availability precluded the inclusion of this approach in the current study, we consider this an important direction for future research to more comprehensively investigate the role of TRPM8 in neuronal excitability and activity.

## Conclusions

In conclusion, this study demonstrates that cortical TRPM8 activation enhances susceptibility to SD, and trigeminal TRPM8 activation induces CGRP-associated effects and neuroinflammation, providing insights into the contributing role of TRPM8 in migraine pathophysiology.

## Abbreviations

AP	Anteroposterior
BK channels	Large-conductance Ca <sup>2+</sup> -activated K <sup>+</sup> channels
CaMKII	Calcium/calmodulin-dependent protein kinase II
CGRP	Calcitonin gene-related peptide
Cox2	Cyclooxygenase 2
Cre	Cre-recombinase
DMEM	Dulbecco's modified eagle medium
DMSO	Dimethyl sulfoxide
DRG	Dorsal root ganglia
EGFP	Enhanced green fluorescent protein
ELISA	Enzyme-linked immunosorbent assay
GWAS	Genome-wide association studies
i.c.v.	Intracerebroventricular
KCl	Potassium chloride
ML	Mediolateral
NTG	Nitroglycerin
PANX1	Pannexin 1
PBS	Phosphate-buffered saline
PIP2	Phosphatidylinositol-4,5-bisphosphate (PIP2)
PKC	Protein kinase C
SD	Spreading depolarization
SNP	Single nucleotide polymorphism
TCC	Trigemino-cervical complex
TG	Trigeminal ganglia
TNC	Trigeminal nucleus caudalis
TRPA1	Transient receptor potential ankyrin 1
TRPM8	Transient receptor potential melastatin 8
TRPV1	Transient receptor potential vanilloid 1
TVS	Trigeminovascular system

## Supplementary Information

The online version contains supplementary material available at <https://doi.org/10.1186/s10194-025-01997-2>.

Supplementary Material 1

Supplementary Material 2

Supplementary Material 3

Supplementary Material 4

Supplementary Material 5

### Acknowledgements

We express our gratitude to Chen-Jee Hong, MD, for his guidance in establishing the primary TG culture, and to Pei-Chun Wu, PhD, for her technical assistance in measuring intracellular calcium concentration.

### Author contributions

Tzu-Ting Liu performed the acquisition of immunofluorescence images, conducted data analysis and interpretation, and contributed to drafting the manuscript. Pin-Yu Chen assisted in manuscript preparation. Chyun-Yea Tseng conducted the SD model-related experiments, performed immunohistochemistry imaging, and managed data acquisition. Yun-Ning Chen and Jian Bang Chen established the primary TG culture, conducted related experiments, and acquired the data. Tz-Han Ni performed immunofluorescence staining. Shuu-Jiun Wang provided critical revisions to enhance the manuscript's intellectual rigor. Shih-Pin Chen conceived and designed the study, providing critical revisions for significant intellectual content. Jiin-Cherng Yen contributed to the study's conceptualization and design, and supervised the research. All authors reviewed and approved the final manuscript.

### Funding

This work was funded by research grant from Ministry of Science and Technology of Taiwan [MOST 110-2314-B-A49A-544; 111-2314-B-A49-070-MY3 (to JCY); the National Science and Technology Council, Taiwan [NSTC 110-2326-B-A49A-501 -MY3 & 112-2314-B-A49 -037 -MY3 (SPC); NSTC 110-2321-B-010-005, 111-2321-B-A49-004, 111-2314-B-075 -086 -MY3, 111-2321-B-A49-011, and 112-2321-B-075-007 (SJW)]; Ministry of Health and Welfare, Taiwan [MOHW112-TDU-B-211-144001] (SJW); Taipei Veterans General Hospital, Taiwan [V113C-120 & V113E004-1 (SJW); V111C-158, V112C-053, V112D67-001-MY3-2 & V113C-058 (SPC)], and the Brain Research Center, National Yang-Ming University, from The Featured Areas Research Center Program within the framework of the Higher Education Sprout Project by the Ministry of Education in Taiwan (to SPC); This work is particularly supported by "Yin Yen-Liang Foundation Development and Construction Plan" of the College of Medicine, National Yang Ming Chiao Tung University.

### Data availability

Raw data inquiries are available from the corresponding author upon reasonable request.

### Declarations

#### Ethics approval

All procedures were conducted following the approval of the Institutional Animal Care and Use Committee of National Yang Ming Chiao Tung University, Taiwan.

#### Consent for publication

Not applicable.

#### Competing interests

The authors declare no competing interests.

#### Author details

<sup>1</sup>Brain Research Center, National Yang Ming Chiao Tung University, Taipei 112, Taiwan

<sup>2</sup>Institute of Pharmacology, College of Medicine, National Yang Ming Chiao Tung University, 5th floor, Shouren Building, No. 155, Sec. 2, Linong St., Beitou District, Taipei 112, Taiwan

<sup>3</sup>Institute of Clinical Medicine, College of Medicine, National Yang Ming Chiao Tung University, Taipei 112, Taiwan

<sup>4</sup>Faculty of Medicine, College of Medicine, National Yang Ming Chiao Tung University, Taipei 112, Taiwan

<sup>5</sup>Department of Neurology, Neurological Institute, Taipei Veterans General Hospital, Taipei 112201, Taiwan

<sup>6</sup>Division of Translational Research, Department of Medical Research, Taipei Veterans General Hospital, Taipei 11217, Taiwan

Received: 13 September 2024 / Accepted: 9 March 2025

Published online: 14 March 2025

### References

1. Global burden of 369 diseases and injuries in 204 countries and territories, 1990–2019: a systematic analysis for the global burden of disease study 2019. *Lancet* 396(10258):1204–1222. [https://doi.org/10.1016/s0140-6736\(20\)30925-9](https://doi.org/10.1016/s0140-6736(20)30925-9)
2. Steiner TJ, Stovner LJ (2023) Global epidemiology of migraine and its implications for public health and health policy. *Nat Rev Neurol* 19(2):109–117. <https://doi.org/10.1038/s41582-022-00763-1>
3. Chasman DI, Schürks M, Anttila V, de Vries B, Schminke U, Launer LJ et al (2011) Genome-wide association study reveals three susceptibility loci for common migraine in the general population. *Nat Genet* 43(7):695–698. <https://doi.org/10.1038/ng.856>
4. Freilinger T, Anttila V, de Vries B, Malik R, Kallela M, Terwindt GM et al (2012) Genome-wide association analysis identifies susceptibility loci for migraine without aura. *Nat Genet* 44(7):777–782. <https://doi.org/10.1038/ng.2307>
5. Ling YH, Chen SP, Fann CS, Wang SJ, Wang YF (2019) TRPM8 genetic variant is associated with chronic migraine and allodynia. *J Headache Pain* 20(1):115. <https://doi.org/10.1186/s10194-019-1064-2>
6. Gavva NR, Sandrock R, Arnold GE, Davis M, Lamas E, Lindvay C et al (2019) Reduced TRPM8 expression underpins reduced migraine risk and attenuated cold pain sensation in humans. *Sci Rep* 9(1):19655. <https://doi.org/10.1038/s41598-019-56295-0>
7. Dhaka A, Earley TJ, Watson J, Patapoutian A (2008) Visualizing cold spots: TRPM8-expressing sensory neurons and their projections. *J Neurosci* 28(3):566–575. <https://doi.org/10.1523/jneurosci.3976-07.2008>
8. Takashima Y, Daniels RL, Knowlton W, Teng J, Liman ER, McKemy DD (2007) Diversity in the neural circuitry of cold sensing revealed by genetic axonal labeling of transient receptor potential melastatin 8 neurons. *J Neurosci* 27(51):14147–14157. <https://doi.org/10.1523/jneurosci.4578-07.2007>
9. Ren L, Dhaka A, Cao YQ (2015) Function and postnatal changes of dorsal afferent fibers expressing TRPM8 channels. *Mol Pain* 11:37. <https://doi.org/10.1186/s12990-015-0043-0>
10. Fedinec AL, Liu J, Zhang R, Harsono M, Pourcyrous M, Parfenova H (2021) The cold receptor TRPM8 activation leads to attenuation of endothelium-dependent cerebral vascular functions during head cooling. *J Cereb Blood Flow Metab* 41(11):2897–2906. <https://doi.org/10.1177/0271678x211018035>
11. Ordás P, Hernández-Ortego P, Vara H, Fernández-Peña C, Reimúndez A, Morenilla-Palao C et al (2021) Expression of the cold thermoreceptor TRPM8 in rodent brain thermoregulatory circuits. *J Comp Neurol* 529(1):234–256. <https://doi.org/10.1002/cne.24694>
12. Ashina M, Hansen JM, Do TP, Melo-Carrillo A, Burstein R, Moskowitz MA (2019) Migraine and the trigeminovascular system—40 years and counting. *Lancet Neurol* 18(8):795–804. [https://doi.org/10.1016/s1474-4422\(19\)30185-1](https://doi.org/10.1016/s1474-4422(19)30185-1)
13. Hoffmann J, Lo H, Neeb L, Martus P, Reuter U (2011) Weather sensitivity in migraineurs. *J Neurol* 258(4):596–602. <https://doi.org/10.1007/s00415-010-5798-7>
14. Mattsson P (2001) Headache caused by drinking cold water is common and related to active migraine. *Cephalalgia* 21(3):230–235. <https://doi.org/10.1046/j.1468-2982.2001.00211.x>
15. Selekler HM, Erdogan MS, Budak F (2004) Prevalence and clinical characteristics of an experimental model of 'ice-cream headache' in migraine and episodic tension-type headache patients. *Cephalalgia* 24(4):293–297. <https://doi.org/10.1111/j.1468-2982.2004.00674.x>
16. Kraya T, Schulz-Ehlbeck M, Burow P, Watzke S, Zierz S (2020) Prevalence and characteristics of headache attributed to ingestion or inhalation of a cold stimulus (HICS): a cross-sectional study. *Cephalalgia* 40(3):299–306. <https://doi.org/10.1177/0333102419884938>
17. Burgos-Vega CC, Ahn DD, Bischoff C, Wang W, Horne D, Wang J et al (2016) Meningeal transient receptor potential channel M8 activation causes cutaneous facial and hindpaw allodynia in a preclinical rodent model of headache. *Cephalalgia* 36(2):185–193. <https://doi.org/10.1177/0333102415584313>

18. Wei C, Kim B, McKemy DD (2022) Transient receptor potential melastatin 8 is required for nitroglycerin- and calcitonin gene-related peptide-induced migraine-like pain behaviors in mice. *Pain* 163(12):2380–2389. <https://doi.org/10.1097/j.pain.0000000000002635>
19. Ucler S, Coskun O, Inan LE, Kanatli Y (2006) Cold therapy in migraine patients: open-label, non-controlled, pilot study. *Evid Based Complement Alternat Med* 3(4):489–493. <https://doi.org/10.1093/ecam/nel035>
20. Sprouse-Blum AS, Gabriel AK, Brown JP, Yee MH (2013) Randomized controlled trial: targeted neck cooling in the treatment of the migraine patient. *Hawaii J Med Public Health* 72(7):237–241
21. Vanderpol J, Bishop B, Matharu M, Glencorse M (2015) Therapeutic effect of intranasal evaporative cooling in patients with migraine: a pilot study. *J Headache Pain* 16:5. <https://doi.org/10.1186/1129-2377-16-5>
22. Borhani Haghighi A, Motazedian S, Rezaii R, Mohammadi F, Salarian L, Pourmokhtari M et al (2010) Cutaneous application of menthol 10% solution as an abortive treatment of migraine without aura: a randomised, double-blind, placebo-controlled, crossed-over study. *Int J Clin Pract* 64(4):451–456. <https://doi.org/10.1111/j.1742-1241.2009.02215.x>
23. Kayama Y, Shibata M, Takizawa T, Iбата K, Shimizu T, Ebine T et al (2018) Functional interactions between transient receptor potential M8 and transient receptor potential V1 in the trigeminal system: relevance to migraine pathophysiology. *Cephalalgia* 38(5):833–845. <https://doi.org/10.1177/0333102417712719>
24. Alarcón-Alarcón D, Cabañero D, de Andrés-López J, Nikolaeva-Koleva M, Giorgi S, Fernández-Ballester G et al (2022) TRPM8 contributes to sex dimorphism by promoting recovery of normal sensitivity in a mouse model of chronic migraine. *Nat Commun* 13(1):6304. <https://doi.org/10.1038/s41467-022-33835-3>
25. Hadjikhani N, Sanchez Del Rio M, Wu O, Schwartz D, Bakker D, Fischl B et al (2001) Mechanisms of migraine aura revealed by functional MRI in human visual cortex. *Proc Natl Acad Sci U S A* 98(8):4687–4692. <https://doi.org/10.1073/pnas.071582498>
26. Ayata C (2009) Spreading depression: from serendipity to targeted therapy in migraine prophylaxis. *Cephalalgia* 29(10):1095–1114. <https://doi.org/10.1111/j.1468-2982.2009.01982.x>
27. Bolay H, Reuter U, Dunn AK, Huang Z, Boas DA, Moskowitz MA (2002) Intrinsic brain activity triggers trigeminal meningeal afferents in a migraine model. *Nat Med* 8(2):136–142. <https://doi.org/10.1038/nm0202-136>
28. Zhang X, Levy D, Noseda R, Kainz V, Jakubowski M, Burstein R (2010) Activation of meningeal nociceptors by cortical spreading depression: implications for migraine with aura. *J Neurosci* 30(26):8807–8814. <https://doi.org/10.1523/Jneurosci.0511-10.2010>
29. Zhang X, Levy D, Kainz V, Noseda R, Jakubowski M, Burstein R (2011) Activation of central trigeminovascular neurons by cortical spreading depression. *Ann Neurol* 69(5):855–865. <https://doi.org/10.1002/ana.22329>
30. Wang Y, Tye AE, Zhao J, Ma D, Raddant AC, Bu F et al (2019) Induction of calcitonin gene-related peptide expression in rats by cortical spreading depression. *Cephalalgia* 39(3):333–341. <https://doi.org/10.1177/0333102416678388>
31. Liu TT, Chen SP, Wang SJ, Yen JC (2024) Vagus nerve stimulation inhibits cortical spreading depression via glutamate-dependent TrkB activation mechanism in the nucleus tractus solitarius. *Cephalalgia* 44(2):3331024241230466. <https://doi.org/10.1177/03331024241230466>
32. Morais A, Liu TT, Qin T, Sadhegiani H, Ay I, Yagmur D et al (2020) Vagus nerve stimulation inhibits cortical spreading depression exclusively through central mechanisms. *Pain* 161(7):1661–1669. <https://doi.org/10.1097/j.pain.0000000000001856>
33. Liu TT, Morais A, Takizawa T, Mulder I, Simon BJ, Chen SP et al (2022) Efficacy profile of noninvasive vagus nerve stimulation on cortical spreading depression susceptibility and the tissue response in a rat model. *J Headache Pain* 23(1):12. <https://doi.org/10.1186/s10194-022-01384-1>
34. Beaudoin GM 3rd, Lee SH, Singh D, Yuan Y, Ng YG, Reichardt LF, Arikath J (2012) Culturing pyramidal neurons from the early postnatal mouse hippocampus and cortex. *Nat Protoc* 7(9):1741–1754. <https://doi.org/10.1038/nprot.2012.099>
35. Wu PC, Kao LS (2016) Calcium regulation in mouse mesencephalic neurons—differential roles of Na(+)/Ca(2+) exchanger, mitochondria and endoplasmic reticulum. *Cell Calcium* 59(6):299–311. <https://doi.org/10.1016/j.ceca.2016.03.008>
36. Chen PY, Yen JC, Liu TT, Chen ST, Wang SJ, Chen SP (2023) Neuronal NLRP3 inflammasome mediates spreading depolarization-evoked trigeminovascular activation. *Brain* 146(7):2989–3002. <https://doi.org/10.1093/brain/awad045>
37. Metgud R, Astekar MS, Soni A, Naik S, Vanishree M (2013) Conventional xylene and xylene-free methods for routine histopathological preparation of tissue sections. *Biotech Histochem* 88(5):235–241. <https://doi.org/10.3109/10520295.2013.764015>
38. Kielkopf CL, Bauer W, Urbatsch IL (2020) Bradford assay for determining protein concentration. *Cold Spring Harb Protoc* 2020(4):102269. <https://doi.org/10.1101/pdb.prot102269>
39. Karatas H, Erdener SE, Gursoy-Ozdemir Y, Lule S, Eren-Koçak E, Sen ZD, Dalkara T (2013) Spreading depression triggers headache by activating neuronal Panx1 channels. *Science* 339(6123):1092–1095. <https://doi.org/10.1126/science.1231897>
40. Takizawa T, Qin T, Lopes de Morais A, Sugimoto K, Chung JY, Morsett L et al (2020) Non-invasively triggered spreading depolarizations induce a rapid pro-inflammatory response in cerebral cortex. *J Cereb Blood Flow Metab* 40(5):1117–1131. <https://doi.org/10.1177/0271678x19859381>
41. Durham PL, Masterson CG (2013) Two mechanisms involved in trigeminal CGRP release: implications for migraine treatment. *Headache* 53(1):67–80. <https://doi.org/10.1111/j.1526-4610.2012.02262.x>
42. Baccei ML, Bardoni R, Fitzgerald M (2003) Development of nociceptive synaptic inputs to the neonatal rat dorsal horn: glutamate release by capsaicin and menthol. *J Physiol* 549(Pt 1):231–242. <https://doi.org/10.1113/jphysiol.2003.040451>
43. Tsuzuki K, Xing H, Ling J, Gu JG (2004) Menthol-induced Ca<sup>2+</sup> release from presynaptic Ca<sup>2+</sup> stores potentiates sensory synaptic transmission. *J Neurosci* 24(3):762–771. <https://doi.org/10.1523/Jneurosci.4658-03.2004>
44. Wrigley PJ, Jeong HJ, Vaughan CW (2009) Primary afferents with TRPM8 and TRPA1 profiles target distinct subpopulations of rat superficial dorsal horn neurones. *Br J Pharmacol* 157(3):371–380. <https://doi.org/10.1111/j.1476-5381.2009.00167.x>
45. Wondergem R, Bartley JW (2009) Menthol increases human glioblastoma intracellular Ca<sup>2+</sup>, BK channel activity and cell migration. *J Biomed Sci* 16(1):90. <https://doi.org/10.1186/1423-0127-16-90>
46. Karashima Y, Damann N, Prenen J, Talavera K, Segal A, Voets T, Nilius B (2007) Bimodal action of menthol on the transient receptor potential channel TRPA1. *J Neurosci* 27(37):9874–9884. <https://doi.org/10.1523/Jneurosci.2221-07.2007>
47. De Corato A, Lisi L, Capuano A, Tringali G, Tramutola A, Navarra P, Dello Russo C (2011) Trigeminal satellite cells express functional calcitonin gene-related peptide receptors, whose activation enhances interleukin-1 $\beta$  pro-inflammatory effects. *J Neuroimmunol* 237(1–2):39–46. <https://doi.org/10.1016/j.jneuroim.2011.05.013>
48. Peters O, Schipke CG, Hashimoto Y, Kettenmann H (2003) Different mechanisms promote astrocyte Ca<sup>2+</sup> waves and spreading depression in the mouse neocortex. *J Neurosci* 23(30):9888–9896. <https://doi.org/10.1523/Jneurosci.23-30-09888.2003>
49. Footitt DR, Newberry NR (1998) Cortical spreading depression induces an LTP-like effect in rat neocortex in vitro. *Brain Res* 781(1–2):339–342. [https://doi.org/10.1016/S0006-8993\(97\)01359-0](https://doi.org/10.1016/S0006-8993(97)01359-0)
50. Kunkler PE, Kraig RP (2004) P/Q Ca<sup>2+</sup> channel blockade stops spreading depression and related pyramidal neuronal Ca<sup>2+</sup> rise in hippocampal organ culture. *Hippocampus* 14(3):356–367. <https://doi.org/10.1002/hipo.10181>
51. Ayata C, Shimizu-Sasamata M, Lo EH, Noebels JL, Moskowitz MA (2000) Impaired neurotransmitter release and elevated threshold for cortical spreading depression in mice with mutations in the  $\alpha$ 1A subunit of P/Q type calcium channels. *Neuroscience* 95(3):639–645. [https://doi.org/10.1016/S0304-6522\(99\)00446-7](https://doi.org/10.1016/S0304-6522(99)00446-7)
52. van den Maagdenberg AM, Pietrobon D, Pizzorusso T, Kaja S, Broos LA, Cesetti T et al (2004) A Ca $\alpha$ 1a knockin migraine mouse model with increased susceptibility to cortical spreading depression. *Neuron* 41(5):701–710. [https://doi.org/10.1016/S0896-6273\(04\)00085-6](https://doi.org/10.1016/S0896-6273(04)00085-6)
53. Tottene A, Urbani A, Pietrobon D (2011) Role of different voltage-gated Ca<sup>2+</sup> channels in cortical spreading depression: specific requirement of P/Q-type Ca<sup>2+</sup> channels. *Channels (Austin)* 5(2):110–114. <https://doi.org/10.4161/chan.5.2.14149>
54. Lisman J, Schulman H, Cline H (2002) The molecular basis of calcium function in synaptic and behavioural memory. *Nat Rev Neurosci* 3(3):175–190. <https://doi.org/10.1038/nrn753>
55. Kucharz K, Lauritzen M (2018) CaMKII-dependent endoplasmic reticulum fission by whisker stimulation and during cortical spreading depolarization. *Brain* 141(4):1049–1062. <https://doi.org/10.1093/brain/awy036>
56. Sokolov AY, Mengal M, Berkovich R (2024) Menthol dural application alters meningeal arteries tone and enhances excitability of trigeminocervical

- neurons in rats. *Brain Res* 1825:148725. <https://doi.org/10.1016/j.brainres.2023.148725>
57. Citak A, Kilinc E, Torun IE, Ankarali S, Dagistan Y, Yoldas H (2022) The effects of certain TRP channels and voltage-gated KCNQ/Kv7 channel opener retigabine on calcitonin gene-related peptide release in the trigeminovascular system. *Cephalalgia* 42(13):1375–1386. <https://doi.org/10.1177/03331024221114773>
  58. Choi IS, Cho JH, Nakamura M, Jang IS (2021) Menthol facilitates excitatory and inhibitory synaptic transmission in rat medullary dorsal horn neurons. *Brain Res* 1750:147149. <https://doi.org/10.1016/j.brainres.2020.147149>
  59. Abe J, Hosokawa H, Okazawa M, Kandachi M, Sawada Y, Yamanaka K et al (2005) TRPM8 protein localization in trigeminal ganglion and taste papillae. *Brain Res Mol Brain Res* 136(1–2):91–98. <https://doi.org/10.1016/j.molbrainres.2005.01.013>
  60. Peier AM, Moqrich A, Hergarden AC, Reeve AJ, Andersson DA, Story GM et al (2002) A TRP channel that senses cold stimuli and menthol. *Cell* 108(5):705–715. [https://doi.org/10.1016/s0092-8674\(02\)00652-9](https://doi.org/10.1016/s0092-8674(02)00652-9)
  61. Staaf S, Franck MC, Marmigère F, Mattsson JP, Ernfors P (2010) Dynamic expression of the TRPM subgroup of ion channels in developing mouse sensory neurons. *Gene Expr Patterns* 10(1):65–74. <https://doi.org/10.1016/j.gpe.2009.10.003>
  62. Takashima Y, Ma L, McKemy DD (2010) The development of peripheral cold neural circuits based on TRPM8 expression. *Neuroscience* 169(2):828–842. <https://doi.org/10.1016/j.neuroscience.2010.05.039>
  63. Antonopoulos SR, Scharnhorst M, Nalley N, Durham PL (2024) Method for cryopreservation of trigeminal ganglion for establishing primary cultures of neurons and glia. *J Neurosci Methods* 402:110034. <https://doi.org/10.1016/j.jneumeth.2023.110034>
  64. Watt FM (1988) Effect of seeding density on stability of the differentiated phenotype of pig articular chondrocytes in culture. *J Cell Sci* 89(Pt 3):373–378. <https://doi.org/10.1242/jcs.89.3.373>
  65. Gage BK, Webber TD, Kieffer TJ (2013) Initial cell seeding density influences pancreatic endocrine development during in vitro differentiation of human embryonic stem cells. *PLoS ONE* 8(12):e82076. <https://doi.org/10.1371/journal.pone.0082076>
  66. Ghosh S, Dean A, Walter M, Bao Y, Hu Y, Ruan J, Li R (2010) Cell density-dependent transcriptional activation of endocrine-related genes in human adipose tissue-derived stem cells. *Exp Cell Res* 316(13):2087–2098. <https://doi.org/10.1016/j.yexcr.2010.04.015>
  67. Kim DS, Lee MW, Yoo KH, Lee TH, Kim HJ, Jang IK et al (2014) Gene expression profiles of human adipose tissue-derived mesenchymal stem cells are modified by cell culture density. *PLoS ONE* 9(1):e83363. <https://doi.org/10.1371/journal.pone.0083363>
  68. Lee LC, Gadegaard N, de Andrés MC, Turner LA, Burgess KV, Yarwood SJ et al (2017) Nanotopography controls cell cycle changes involved with skeletal stem cell self-renewal and multipotency. *Biomaterials* 116:10–20. <https://doi.org/10.1016/j.biomaterials.2016.11.032>
  69. Andersson DA, Chase HW, Bevan S (2004) TRPM8 activation by menthol, icilin, and cold is differentially modulated by intracellular pH. *J Neurosci* 24(23):5364–5369. <https://doi.org/10.1523/jneurosci.0890-04.2004>
  70. Berridge MJ, Lipp P, Bootman MD (2000) The versatility and universality of calcium signalling. *Nat Rev Mol Cell Biol* 1(1):11–21. <https://doi.org/10.1038/35036035>
  71. Yin Y, Zhang F, Feng S, Butay KJ, Borgnia MJ, Im W, Lee SY (2022) Activation mechanism of the mouse cold-sensing TRPM8 channel by cooling agonist and PIP(2). *Science* 378(6616):eadd1268. <https://doi.org/10.1126/science.add1268>
  72. Premkumar LS, Raisinghani M, Pingle SC, Long C, Pimentel F (2005) Down-regulation of transient receptor potential melastatin 8 by protein kinase C-mediated dephosphorylation. *J Neurosci* 25(49):11322–11329. <https://doi.org/10.1523/jneurosci.3006-05.2005>
  73. Abe J, Hosokawa H, Sawada Y, Matsumura K, Kobayashi S (2006) Ca<sup>2+</sup>-dependent PKC activation mediates menthol-induced desensitization of transient receptor potential M8. *Neurosci Lett* 397(1–2):140–144. <https://doi.org/10.1016/j.neulet.2005.12.005>
  74. Rivera B, Campos M, Orio P, Madrid R, Pertusa M (2020) Negative modulation of TRPM8 channel function by protein kinase C in trigeminal cold thermoreceptor neurons. *Int J Mol Sci* 21(12). <https://doi.org/10.3390/ijms21124420>
  75. Krivanek J, Koroleva VI (1996) Protein kinase C in the rat cerebral cortex during spreading depression. *Neurosci Lett* 210(2):79–82. [https://doi.org/10.1016/0304-3940\(96\)12666-5](https://doi.org/10.1016/0304-3940(96)12666-5)
  76. Toro CA, Eger S, Veliz L, Sotelo-Hitschfeld P, Cabezas D, Castro MA et al (2015) Agonist-dependent modulation of cell surface expression of the cold receptor TRPM8. *J Neurosci* 35(2):571–582. <https://doi.org/10.1523/jneurosci.3820-13.2015>
  77. Chen SP, Qin T, Seidel JL, Zheng Y, Eikermann M, Ferrari MD et al (2017) Inhibition of the P2X7-PANX1 complex suppresses spreading depolarization and neuroinflammation. *Brain* 140(6):1643–1656. <https://doi.org/10.1093/brain/awx085>
  78. Uzay B, Donmez-Demir B, Ozcan SY, Kocak EE, Yemisci M, Ozdemir YG et al (2024) The effect of P2X7 antagonism on subcortical spread of optogenetically-triggered cortical spreading depression and neuroinflammation. *J Headache Pain* 25(1):120. <https://doi.org/10.1186/s10194-024-01807-1>
  79. Nguyen TN, Koga Y, Wakasugi T, Kitamura T, Suzuki H (2023) TRPA1/M8 agonists upregulate ciliary beating through the pannexin-1 channel in the human nasal mucosa. *Mol Biol Rep* 50(3):2085–2093. <https://doi.org/10.1007/s11033-022-08201-7>
  80. Afroz S, Arakaki R, Iwasa T, Oshima M, Hosoki M, Inoue M et al (2019) CGRP induces differential regulation of cytokines from satellite glial cells in trigeminal ganglia and orofacial nociception. *Int J Mol Sci* 20(3). <https://doi.org/10.3390/ijms20030711>
  81. Vause CV, Durham PL (2010) Calcitonin gene-related peptide differentially regulates gene and protein expression in trigeminal glia cells: findings from array analysis. *Neurosci Lett* 473(3):163–167. <https://doi.org/10.1016/j.neulet.2010.01.074>
  82. Afroz S, Arakaki R, Iwasa T, Waskitho A, Oshima M, Matsuya Y (2020) Role of CGRP in neuroimmune interaction via NF- $\kappa$ B signaling genes in glial cells of trigeminal ganglia. *Int J Mol Sci* 21(17). <https://doi.org/10.3390/ijms21176005>
  83. Zakharian E, Cao C, Rohacs T (2010) Gating of transient receptor potential melastatin 8 (TRPM8) channels activated by cold and chemical agonists in planar lipid bilayers. *J Neurosci* 30(37):12526–12534. <https://doi.org/10.1523/jneurosci.3189-10.2010>
  84. Lippoldt EK, Elmes RR, McCoy DD, Knowlton WM, McKemy DD (2013) Artemin, a glial cell line-derived neurotrophic factor family member, induces TRPM8-dependent cold pain. *J Neurosci* 33(30):12543–12552. <https://doi.org/10.1523/jneurosci.5765-12.2013>
  85. Asuthkar S, Demirkhanyan L, Sun X, Elustondo PA, Krishnan V, Baskaran P et al (2015) The TRPM8 protein is a testosterone receptor. II. Functional evidence for an ionotropic effect of testosterone on TRPM8. *J Biol Chem* 290(5):2670–2688. <https://doi.org/10.1074/jbc.M114.610873>
  86. Tang Z, Kim A, Masuch T, Park K, Weng H, Wetzel C, Dong X (2013) Pirt functions as an endogenous regulator of TRPM8. *Nat Commun* 4:2179. <https://doi.org/10.1038/ncomms3179>
  87. Shang H, Wang Y, Chao X, Sun G, Bai X, Xu L et al (2017) Artemin transiently increases iNOS expression in primary cultured trigeminal ganglion neurons. *Neurosci Lett* 660:34–38. <https://doi.org/10.1016/j.neulet.2017.09.016>
  88. Sherkheli MA, Vogt-Eisele AK, Bura D, Beltrán Márquez LR, Gisselmann G, Hatt H (2010) Characterization of selective TRPM8 ligands and their structure activity response (S.A.R) relationship. *J Pharm Pharm Sci* 13(2):242–253. <https://doi.org/10.18433/j3n88n>
  89. Chuang HH, Neuhauser WM, Julius D (2004) The super-cooling agent icilin reveals a mechanism of coincidence detection by a temperature-sensitive TRP channel. *Neuron* 43(6):859–869. <https://doi.org/10.1016/j.neuron.2004.08.038>
  90. Yin Y, Le SC, Hsu AL, Borgnia MJ, Yang H, Lee SY (2019) Structural basis of cooling agent and lipid sensing by the cold-activated TRPM8 channel. *Science* 363(6430). <https://doi.org/10.1126/science.aav9334>
  91. Knowlton WM, Bifolck-Fisher A, Bautista DM, McKemy DD (2010) TRPM8, but not TRPA1, is required for neural and behavioral responses to acute noxious cold temperatures and cold-mimetics in vivo. *Pain* 150(2):340–350. <https://doi.org/10.1016/j.pain.2010.05.021>
  92. Almeida MC, Hew-Butler T, Soriano RN, Rao S, Wang W, Wang J et al (2012) Pharmacological blockade of the cold receptor TRPM8 attenuates autonomic and behavioral cold defenses and decreases deep body temperature. *J Neurosci* 32(6):2086–2099. <https://doi.org/10.1523/jneurosci.5606-11.2012>
  93. Doerner JF, Gisselmann G, Hatt H, Wetzel CH (2007) Transient receptor potential channel A1 is directly gated by calcium ions. *J Biol Chem* 282(18):13180–13189. <https://doi.org/10.1074/jbc.M607849200>
  94. Story GM, Peier AM, Reeve AJ, Eid SR, Mosbacher J, Hricik TR et al (2003) ANKTM1, a TRP-like channel expressed in nociceptive neurons, is activated by cold temperatures. *Cell* 112(6):819–829. [https://doi.org/10.1016/s0092-8674\(03\)00158-2](https://doi.org/10.1016/s0092-8674(03)00158-2)

95. Yarmolinsky DA, Peng Y, Pogorzala LA, Rutlin M, Hoon MA, Zuker CS (2016) Coding and plasticity in the mammalian thermosensory system. *Neuron* 92(5):1079–1092. <https://doi.org/10.1016/j.neuron.2016.10.021>
96. Eikermann-Haerter K, Baum MJ, Ferrari MD, van den Maagdenberg AM, Moskowitz MA, Ayata C (2009) Androgenic suppression of spreading depression in familial hemiplegic migraine type 1 mutant mice. *Ann Neurol* 66(4):564–568. <https://doi.org/10.1002/ana.21779>

### **Publisher's note**

Springer Nature remains neutral with regard to jurisdictional claims in published maps and institutional affiliations.